NASA TECHNICAL NOTE

NASA TN D-7095

NASA TN D-7095

ASYMMETRIC LATERAL-DIRECTIONAL CHARACTERISTICS OF POINTED BODIES OF REVOLUTION AT HIGH ANGLES OF ATTACK

by Paul L. Coe, Jr., Joseph R. Chambers, and William Letko

Langley Research Center
Hampton, Va. 23365

NATIONAL AERONAUTICS AND SPACE ADMINISTRATION • WASHINGTON, D. C. • NOVEMBER 1972

1. Report No.	2. Government Accession No.	3. Recipient's Catalog No.
NASA TN D-7095		

4. Title and Subtitle	5. Report Date
ASYMMETRIC LATERAL-DIRECTIONAL CHARACTERISTICS OF POINTED BODIES OF REVOLUTION AT HIGH ANGLES OF ATTACK	November 1972
	6. Performing Organization Code

7. Author(s)	8. Performing Organization Report No.
Paul L. Coe, Jr.,* Joseph R. Chambers, and William Letko	L-8582
	10. Work Unit No.
9. Performing Organization Name and Address	501-26-04-02
NASA Langley Research Center Hampton, Va. 23365	11. Contract or Grant No.
	13. Type of Report and Period Covered
12. Sponsoring Agency Name and Address	Technical Note
National Aeronautics and Space Administration Washington, D.C. 20546	14. Sponsoring Agency Code

15. Supplementary Notes

*NASA-ASEE summer faculty fellow, 1972; Department of Engineering Sciences, Hofstra University, Long Island, New York

16. Abstract

A low-speed wind-tunnel investigation was conducted in order to determine the cause of asymmetric yawing moments produced by long pointed fuselage nose shapes at high angles of attack. Force tests were conducted with a cone, tangent-ogive model, and a paraboloid of revolution over a range of Reynolds numbers from 0.15×10^6 to 0.35×10^6 for an angle-of-attack range from 0^o to 75^o and an angle-of-sideslip range of $\pm 30^o$. Tuft and smoke flow-visualization tests were also conducted to aid in the analysis. The results of the investigation showed that large asymmetric yawing moments were obtained for the cone and tangent-ogive body at high angles of attack (of the order of 40^o to 60^o). These large moments were caused by asymmetric shedding of vortex sheets off the long pointed nose. The asymmetric moments could be eliminated by use of symmetrically arranged strakes on the nose. The paraboloid of revolution did not produce a strong asymmetric flow field at high angles of attack and did not exhibit asymmetric moments.

17. Key Words (Suggested by Author(s))	18. Distribution Statement
Pointed bodies of revolution Lateral-directional stability	Unclassified – Unlimited

19. Security Classif. (of this report)	20. Security Classif. (of this page)	21. No. of Pages	22. Price*
Unclassified	Unclassified	41	$3.00

*For sale by the National Technical Information Service, Springfield, Virginia 22151

ASYMMETRIC LATERAL-DIRECTIONAL CHARACTERISTICS OF POINTED BODIES OF REVOLUTION AT HIGH ANGLES OF ATTACK

By Paul L. Coe, Jr.,* Joseph R. Chambers,
and William Letko
Langley Research Center

SUMMARY

A low-speed wind-tunnel investigation was conducted in order to determine the cause of asymmetric yawing moments produced by long pointed fuselage nose shapes at high angles of attack. These asymmetric moments are known to have a large influence on the stall and spin characteristics of airplanes. Force tests were conducted with a cone, a tangent-ogive model, and a paraboloid of revolution over a range of Reynolds numbers from 0.15×10^6 to 0.35×10^6 for an angle-of-attack range from 0^o to 75^o and an angle-of-sideslip range of $\pm 30^o$. Tuft and smoke flow-visualization tests were also conducted to aid in the analysis.

The results of the investigation showed that large asymmetric yawing moments were obtained for the cone and tangent ogive at high angles of attack (of the order of 40^o to 60^o). Although the asymmetry for the tangent ogive remained in one direction, the asymmetries obtained for the cone reversed direction as the angle of attack was changed. These large moments were caused by asymmetric shedding of vortex sheets off the long pointed nose. The asymmetric moments could be eliminated by use of symmetrically arranged strakes on the nose. The paraboloid of revolution did not produce a strong asymmetric flow field at high angles of attack and did not exhibit asymmetric moments.

INTRODUCTION

The use of pointed fuselage forebody shapes for present-day supersonic aircraft can have large effects on the stability and control characteristics of these vehicles at high angles of attack. For extremely high angles of attack, such as those angles associated with poststall flight and spins, these shapes have been found (ref. 1) to produce large asymmetric yawing moments which can be much larger than the moments produced by

---

*NASA-ASEE summer faculty fellow, 1972; Department of Engineering Sciences, Hofstra University, Long Island, New York.

deflection of a conventional rudder. These moments may have a predominant effect on stall and spin characteristics and can, in fact, determine the ease and direction in which an airplane may spin. (See ref. 2.) Although the aerodynamic asymmetries produced by sharp noses have been measured during past wind-tunnel investigations of airplane spin characteristics, the basic flow phenomenon is not well understood. As a result, the asymmetries have often either been ignored or have been attributed to poor wind-tunnel flow or significant model asymmetries.

The present investigation was undertaken to (1) determine the fundamental flow phenomenon which produces asymmetries at high angles of attack, (2) illustrate the nature of the asymmetries for three pointed bodies of revolution, and (3) determine the effectiveness of small strakes in eliminating the asymmetries. The investigation was conducted at the Langley Research Center by using three different nose shapes, the tests being conducted in a low-speed wind tunnel having a 3.66-m (12-ft) octagonal test section. An additional limited number of tests were conducted in the 9.1- by 18.3-m (30- by 60-ft) test section of the Langley full-scale tunnel. Static force data were obtained at values of Reynolds numbers of 0.15×10^6, 0.21×10^6, and 0.35×10^6 based on the maximum body diameter. The angle of attack was varied from 0° to 75° and the angle of sideslip was varied from 30° to -30°. Flow over the surface of the bodies was visualized by using wool tufts attached to the bodies. The surrounding flow fields were visualized by using both tuft grid and smoke techniques.

SYMBOLS

The reference-axis system used is illustrated in figure 1. All moments are presented about the reference center shown in figure 2. Dimensional values are given in the International System of Units and the U.S. Customary Units. All longitudinal coefficients are with respect to the wind-axis system. All lateral-directional coefficients are with respect to the body-axis system.

C_D drag coefficient, $\frac{F_D}{q_\infty S_b}$

C_L lift coefficient, $\frac{F_L}{q_\infty S_b}$

C_l rolling-moment coefficient, $\frac{M_X}{q_\infty S_b d}$

C_m pitching-moment coefficient, $\frac{M_Y}{q_\infty S_b d}$

C_n yawing-moment coefficient, $\frac{M_Z}{q_\infty S_b d}$

C_Y side-force coefficient, $\frac{F_Y}{q_\infty S_b}$

d base diameter, m (ft)

F_D drag force, N (lb)

F_L lift force, N (lb)

F_Y side force, N (lb)

M_X rolling moment, m-N (ft-lb)

M_Y pitching moment, m-N (ft-lb)

M_Z yawing moment, m-N (ft-lb)

q_∞ free-stream dynamic pressure, N/m^2 (lb/ft^2)

R Reynolds number

S_b base area, m^2 (ft^2)

X,Y,Z body reference axis, see figure 1

α angle of attack, deg

β angle of sideslip, deg

ϕ angle of inclination of resultant force component in the YZ body plane, measured from vertical, deg

MODELS AND APPARATUS

Models

Sketches of the three bodies of revolution used in the investigation are shown in figure 2. The shapes selected for study were a tangent ogive, a cone, and a paraboloid of revolution; all the bodies had a fineness ratio of 3.5. The models were made of hardwood with a fiber-glass finish and an aluminum nose tip; they were constructed to a tolerance of ±0.013 cm (±0.005 in.) to minimize any effect of geometric asymmetry. A

cylindrical afterbody 53.34 cm (21 in.) long with a diameter of 15.24 cm (6 in.) was also used in a limited number of tests with the tangent-ogive model. The effectiveness of strakes placed 2.54 cm (1.00 in.) aft of the nose tip and symmetrically in the XY-plane of the model was evaluated. (See fig. 1.) The strakes were 1.27 cm (0.5 in.) wide by 8.89 cm (3.50 in.) long.

Wind Tunnels

The investigation was conducted in a low-speed wind tunnel with a 3.66-m (12-ft) octagonal test section at the Langley Research Center and in the 9.1- by 18.3-m (30- by 60-ft) test section of the Langley full-scale tunnel. The models were sting mounted and data were measured with a conventional strain-gage balance.

TESTS

Force Tests

Static force tests were conducted in the low-speed wind tunnel at Reynolds numbers of 0.21×10^6 and 0.15×10^6 based on the maximum body diameter. During the tests, measurements were made of the three lateral-directional force and moment components.

The tests of the bodies in the Langley full-scale tunnel were conducted at a Reynolds number of 0.35×10^6 based on the maximum body diameter. During these tests, simultaneous measurements were made of the six longitudinal and lateral-directional force and moment components. In all tests the angle of attack varied from 0° to 75° for a range of angles of sideslip of $\pm 30^\circ$.

Flow-Visualization Tests

Flow-visualization tests were conducted to define the flow field on the surface, and in the vicinity of the models. The tests were performed by using tufts on the surfaces of the models, a tuft grid placed slightly behind the models, and smoke techniques. The angle of attack for the visualization tests ranged from 0° to 75° for a range of angles of sideslip of $\pm 30^\circ$.

DESCRIPTION OF THE FLOW PHENOMENA PRODUCING ASYMMETRIES AT HIGH ANGLES OF ATTACK

The results of past investigations such as those of reference 1 have indicated that the large asymmetric yawing moments produced by long pointed fuselage forebodies are caused by asymmetric shedding of vortex sheets from the nose. As shown in figure 3 (taken from ref. 1), flow separation on a long nose at zero sideslip tends to produce a

symmetrical pattern of vortex sheets at low angles of attack. This symmetrical flow pattern does not produce any side force on the nose; and, as a result, there is no yawing moment produced. At a higher angle of attack, however, the vortices increase in strength; the flow pattern becomes asymmetrical; and a side force is produced on the nose which, in turn, produces a yawing moment about the airplane center of gravity. The results of the present investigation agreed with this description and provided information toward a better understanding of the phenomena.

RESULTS AND DISCUSSION

The results of the present investigation are discussed for each of the individual body shapes tested. Longitudinal and lateral-directional aerodynamic characteristics and flow-visualization results are presented.

Results for Tangent-Ogive Body

Longitudinal characteristics.- The longitudinal aerodynamic characteristics obtained for the tangent-ogive model at zero sideslip are presented in figure 4. The most important characteristics to be noted are that the tangent-ogive model produced a nonlinear variation of lift coefficient with angle of attack and that the maximum value of the lift coefficient was obtained at an angle of attack of 50°.

Lateral-directional characteristics.- The variation with angle of attack of the lateral-directional aerodynamic characteristics obtained for the tangent-ogive model at zero sideslip are presented in figure 5. Data are presented for the basic body in the Langley full-scale tunnel ($R = 0.35 \times 10^6$) and in the low-speed tunnel ($R = 0.15 \times 10^6$ and $R = 0.21 \times 10^6$). In addition, data are presented for the tangent-ogive body with a 53.34-cm (21-in.) cylindrical afterbody added. When the afterbody was added, the moment reference center remained in the same position relative to the base of the tangent-ogive model, that is, most of the afterbody was behind the moment reference center. The data show that the basic tangent-ogive model experienced no significant values of yawing moment at zero sideslip for low angles of attack, as might be expected. For values of α greater than 40°, however, large asymmetric values of C_n and C_Y were measured. The asymmetries reached maximum values near $\alpha = 55^{\circ}$ and decreased to near zero values at approximately $\alpha = 65^{\circ}$. It was found that the data were repeatable to within ± 5 percent, and no hysteresis effects were found.

It is important to note that the asymmetric values of C_n were primarily positive or nose right in sense. These nose-right moments were accompanied by positive values of C_Y (side force to the right). This relationship is an indication of the potential of large side forces on an airplane nose to cause large asymmetric yawing moments at high angles of attack.

The data obtained for the tangent ogive with a cylindrical afterbody showed generally larger values of C_n and C_Y than those values obtained for the basic body. This result was probably caused by the flow field acting on the additional area provided by the afterbody.

The results of additional tests conducted to determine the effects of reorienting the body of revolution about the longitudinal axis are presented in figure 6. Data are shown for the basic model (0^o orientation) and for the model rotated 90^o, 180^o, and 270^o about the X body axis. The data show that asymmetric values of C_n were produced in both directions and that the magnitudes of the moments were approximately the same in either direction. This effect was due to the fact that the body was not perfectly symmetrical.

The results of tuft flow-visualization tests conducted for the tangent-ogive model at zero sideslip are shown in figure 7. The photographs shown at the top of the figure illustrate the flow over the surface of the model whereas the lower photographs show the flow pattern with a tuft grid held at the base of the model. The photographs for $\alpha = 5^o$ show a symmetrical flow pattern on and about the model with no significant vortex formation. For $\alpha = 30^o$, the tufts indicate that two symmetrical vortex sheets exist, similar to those shown for low angles of attack in figure 3. At $\alpha = 55^o$, where the model experienced a maximum asymmetric value of C_n to the right (see fig. 5), the tufts show that an asymmetrical pattern of vortex sheets was shed by the model, similar to those indicated by the sketch of figure 3. One relatively small vortex core was displaced high above and to the left of the model, whereas a large vortex core was located slightly above and to the right of the model. The flow pattern was relatively invariant with time. Although no pressure measurements were made in the present investigation, the data indicate that the large vortex core remains close to the body. The resulting vortex-induced flow impinges on the body and creates a side force to the right.

Another study was made with a tuft grid to determine the extent to which the flow pattern enveloped the body. The results of these tests, shown in figure 8, show the flow pattern on the tangent-ogive model (with a cylindrical afterbody added) at several stations downstream of the model. The data show that a large area above the model was affected by the flow and that the small vortex core remained in about the same location as the tuft grid was moved downstream. The large vortex core, however, appeared to grow in size and follow the upper surface of the model at downstream stations.

An example of the correlation of the foregoing results with those obtained for conventional airplane configurations is presented in figure 9. In figure 9 the vortex sheets have been further defined by use of smoke. The photograph shown in the upper part of the figure shows the tangent-ogive model of the present investigation at $\alpha = 55^o$, $\beta = 0^o$. The photograph in the lower part of the figure shows similar results obtained for the model of reference 1 at $\alpha = 60^o$, $\beta = 0^o$. Both models exhibited large positive asym-

metric values of C_n for these test conditions. The flow patterns about the models are very similar in nature. In particular, the small vortex core is seen to separate near the nose of the model and trail horizontally downstream whereas the large vortex core remains close to the body and extends a considerable length from the nose tip.

An interesting measure of the degree of asymmetry induced by the flow field shown in the previous photographs is afforded by consideration of the inclination of the resultant force within the YZ-plane of the model. Shown in figure 10 is the inclination of resultant force obtained by adding vectorially the side-force and normal-force coefficients at $\beta = 0^o$. The data show that the resultant force was inclined over 40^o from the vertical near $\alpha = 55^o$.

All the foregoing force tests and flow-visualization tests were conducted for $\beta = 0^o$. The effects of sideslipping the model were measured for $\alpha = 0^o$, 30^o, and 55^o and the results are presented in figure 11. For $\alpha = 0^o$ and 30^o, the model was directionally unstable about the moment reference center, and the variations of C_n and C_Y with β were fairly linear. For $\alpha = 55^o$, the model exhibited the large asymmetries previously noted, and the variations of C_n and C_Y with β were linear over most of the range of sideslip. One remarkable result shown by the data is that the model exhibited positive values of C_n for values of β of over 30^o. Apparently, the large angle of inclination of the resultant force shown in figure 10 persisted for large values of β.

The results of flow-visualization tests for several values of β are shown in figure 12. For $\alpha = 5^o$ and $\alpha = 30^o$, the flow patterns are symmetrical as would be expected. For $\alpha = 55^o$, the flow patterns obtained over a range of sideslip of $\pm 20^o$ appear to be relatively independent of sideslip; this result correlates well with the results of the force tests.

Results for Cone

Longitudinal characteristics.- The longitudinal characteristics obtained for the cone at zero sideslip are presented in figure 13. The maximum value of C_L for the cone occurred near an angle of attack of 55^o.

Lateral-directional characteristics.- The variation of the lateral-directional characteristics with angle of attack for the cone at zero sideslip is presented in figure 14. These data were measured in both wind tunnels as was the case for the tangent-ogive model. The data of figure 14 show that the cone also exhibited large asymmetric yawing moments at high angles of attack. One distinctive characteristic of the cone, however, was the fact that the asymmetries reversed direction as α was increased. The results shown were found to be repeatable with no noticeable hysteresis effect.

Presented in figure 14(b) are the results of additional tests conducted to determine the effects of reorienting the cone. The results show that similar data were obtained for

rotation angles of 0°, 180°, and 270°, but a rotation angle of 90° produced a reversal in the sense of the asymmetries, the magnitudes of the asymmetries and the angle of attack at which they occurred remaining relatively unchanged.

The results of tuft flow-visualization tests for the cone at zero sideslip are shown in figure 15. The photographs shown in figure 15(a) show the flow over the top of the model for increasing values of α at zero sideslip. The photographs show that symmetrical flow existed over the model for values of α up to 25°. For angles of attack greater than 25°, the tufts indicate that an asymmetric flow pattern existed, particularly along the center of the upper surface. The data show that the asymmetric flow pattern tended to change direction as α was varied, and this result correlates with the force-test data shown in figure 14 in the same manner as the data for the tangent-ogive model. Additional information regarding the flow field shed from the model was provided by the tuft grid photographs shown in figure 15(b). These photographs showed that a flow field similar to that observed for the tangent-ogive body also existed for the cone; that is, a small vortex core was identified near the nose, and a larger vortex core was located near the upper surface of the model. As the angle of attack of the cone was varied, however, the two vortices tended to exchange positions on either side of the cone. For example, at $\alpha = 40^{\circ}$ the smaller vortex core appears to the left of the model and the larger core appears to the right; this pattern resulted in impingement of the vortex flow on the cone, and a resultant nose-right yawing moment, as shown in figure 14. At $\alpha = 50^{\circ}$, the vortex cores moved to opposite sides of the model; this flow pattern resulted in a nose-left value of yawing moment.

The inclination of the resultant force acting in the YZ-plane as a function of angle of attack is presented, for the cone, in figure 16. The resultant force was inclined at angles of up to approximately 40° from the vertical, and the variations in the flow with angle of attack resulted in fluctuations of the force from side to side at high angles of attack.

The effects of sideslipping the cone are shown in figure 17 for angles of attack of 0° (no asymmetry at $\beta = 0^{\circ}$), 40° (nose-right asymmetry at $\beta = 0^{\circ}$), and 50° (nose-left asymmetry at $\beta = 0^{\circ}$). The model was, in general, directionally unstable at the angles of attack of the tests. The asymmetric values of C_n were nulled by sideslipping the model to a β approximately equal to 15°.

Results for Paraboloid of Revolution

Longitudinal characteristics.- The longitudinal aerodynamic characteristics of the paraboloid of revolution are compared with the characteristics of the tangent-ogive body and cone in figure 18. The data show that the paraboloid and tangent-ogive body had similar lift characteristics over the angle-of-attack range of the tests.

Lateral-directional characteristics.- The variation of the lateral-directional characteristics of the paraboloid with angle of attack at $\beta = 0^{o}$ is compared, in figure 19, with those measured for the tangent-ogive model and cone. The data show that the paraboloid model had no significant asymmetries whereas the other two models did.

The results of the flow-visualization tests for the paraboloid of revolution are presented in figure 20 which shows the flow on the surface of the model for various sideslip angles at angles of attack of 5^{o}, 30^{o}, and 55^{o}. The flow was characterized by two shed vortex sheets which remained in a symmetrical position as α was increased.

At angles of attack of 5^{o} and 30^{o}, the flow pattern is symmetrical over the sideslip range in a manner similar to that exhibited by the tangent-ogive model shown in figure 12(a). However, for $\alpha = 55^{o}$, the asymmetric flow pattern of the tangent-ogive model was not exhibited by the paraboloid of revolution. Apparently, the relatively symmetrical flow pattern shown by the paraboloid did not create significant yawing moments.

The relatively symmetrical nature of the flow about the paraboloid is illustrated by the data of figure 21 which shows the inclination of the resultant force vector within the YZ body plane as a function of the angle of attack. The data show that the inclination of the force vector was small over the entire range of angle of attack. This result was caused by the fact that the paraboloid exhibited a symmetrical flow field and no appreciable side force at 0^{o} sideslip.

The effect of sideslip on the lateral-directional characteristics of the paraboloid is shown in figure 22. The data show that for $\alpha = 0^{o}$ and 30^{o}, the model was directionally unstable and the variations of C_n and C_Y with β were approximately linear. For $\alpha = 55^{o}$, the model was generally unstable and significant nonlinearities existed in the data over the range of sideslip.

Effects of Strakes

Past investigations (ref. 2, for example) have shown that small strakes placed near the tip of the nose of a pointed body can eliminate, or minimize, large asymmetric yawing moments at high angles of attack. A series of tests were therefore conducted to determine the effectiveness of strakes for the tangent-ogive body and the cone of the present investigation. The strakes tested were placed symmetrically in the XY-plane of the model.

Longitudinal characteristics.- The effect of the strakes on the longitudinal characteristics of the tangent-ogive model and the cone are shown in figure 23. The data of figure 23 show that the addition of the strakes to the tangent-ogive model slightly reduce the magnitude of C_L for angles of attack greater than 45^{o}.

Lateral-directional characteristics.- The results obtained for the tangent-ogive model and cone with the strakes added are shown in figure 24. The data show that the strakes virtually eliminated the asymmetries obtained for the tangent-ogive model and significantly reduced those for the cone. The effect of the strakes was to produce a well-defined point of separation which resulted in a symmetrical flow field at all angles of attack. This result is evidenced by figure 25 which shows the flow field behind the tangent-ogive model with the strakes, to be very similar to the flow field behind the paraboloid of revolution.

SUMMARY OF RESULTS

A low-speed wind-tunnel investigation was conducted to provide fundamental information regarding the cause and potential cures for the large asymmetric yawing moments created by pointed fuselages at high angles of attack. The results relative to the effects of body shape and the use of strakes on the aerodynamics of pointed bodies are as follows:

1. The tangent ogive and cone exhibited large asymmetric yawing moments at high angles of attack (of the order of 40^{o} to 60^{o}).

2. The yawing moments were caused by asymmetric shedding of vortex sheets off the long pointed noses.

3. The asymmetric yawing moments were eliminated by the use of symmetrically placed strakes on the nose.

4. The asymmetry for the tangent-ogive model remained in one direction whereas the asymmetry for the cone reversed direction as the angle of attack changed.

5. The paraboloid of revolution did not produce a strong asymmetric flow field at high angles of attack and did not exhibit asymmetric moments.

It should be recognized, however, that other factors such as Reynolds number, nose protuberances (such as nose booms), and wing-fuselage interference effects may alter some of the trends indicated. In addition, the cross-sectional shapes of the nose may cause significant differences on the effect of sideslip angle at high angles of attack.

Langley Research Center,
National Aeronautics and Space Administration,
Hampton, Va., October 18, 1972.

REFERENCES

1. Chambers, Joseph R.; Anglin, Ernie L.; and Bowman, James S., Jr.: Effects of a Pointed Nose on Spin Characteristics of a Fighter Airplane Model Including Correlation With Theoretical Calculations. NASA TN D-5921, 1970.

2. Neihouse, Anshal I.; Klinar, Walter J.; and Scher, Stanley H.: Status of Spin Research for Recent Airplane Designs. NASA TR R-57, 1960. (Supersedes NACA RM L57F12.)

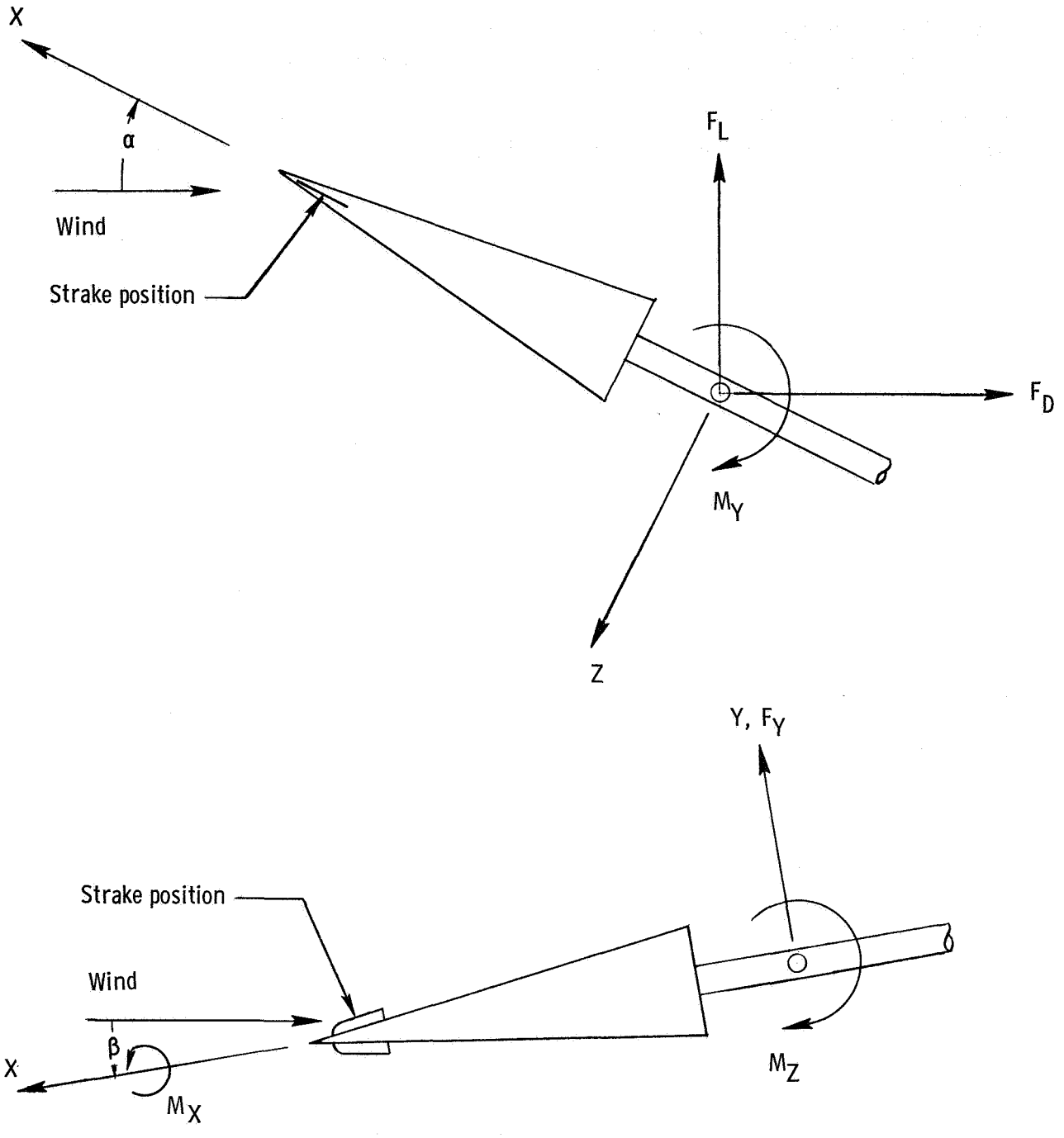

Figure 1.- Axis system used in the investigation.

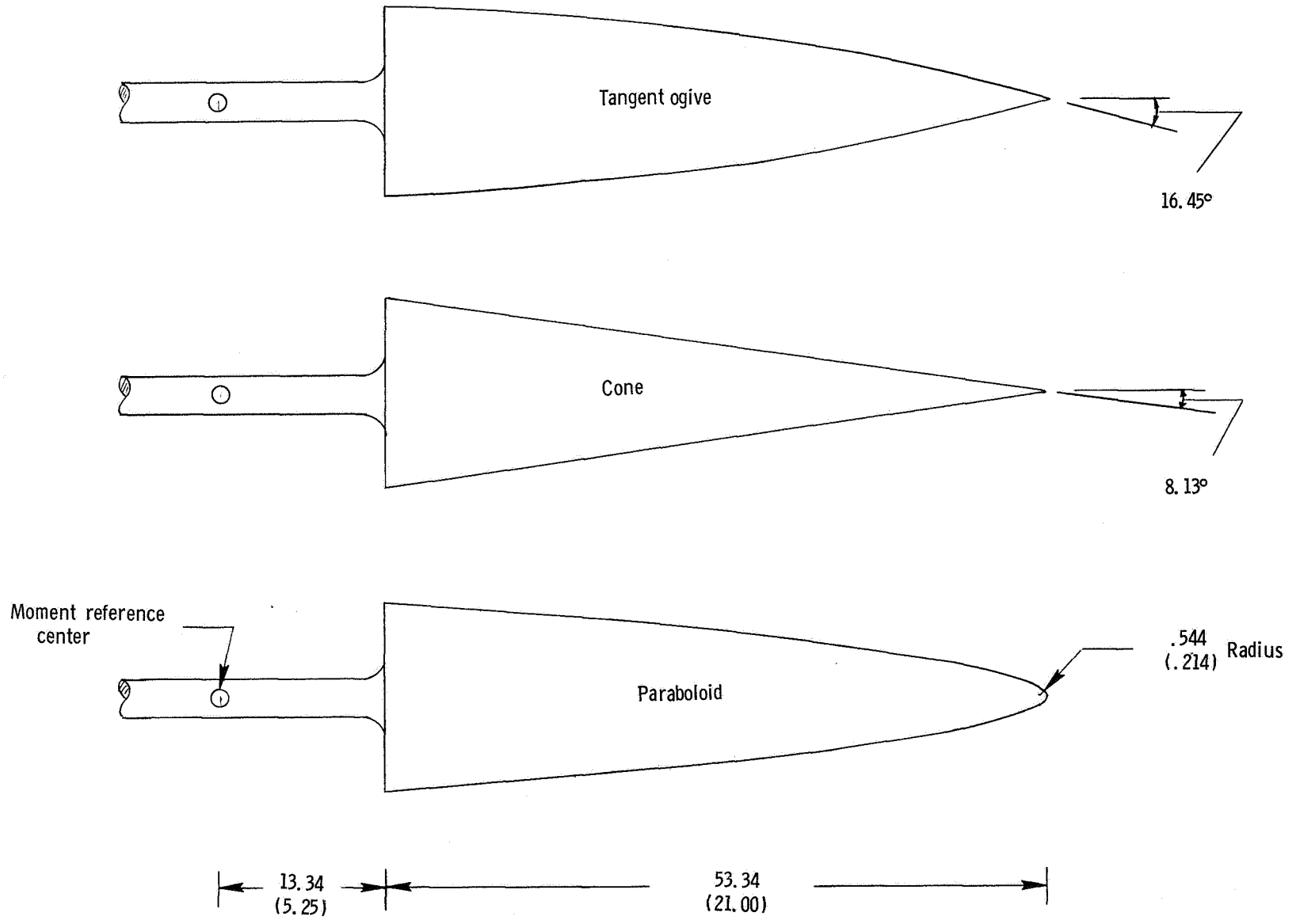

Figure 2.- Sketches of the models used. Dimensions are given in centimeters and parenthetically in inches. Base diameter, 15.24 cm (6 in.); base area, 182.42 cm^2 (28.27 in^2); fineness ratio, 3.5.

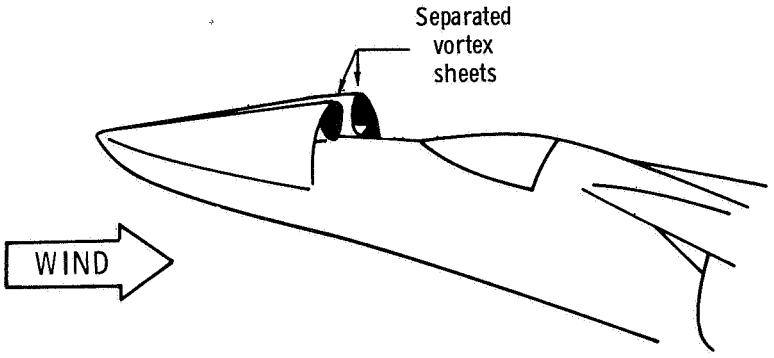

(a) Low angles of attack.

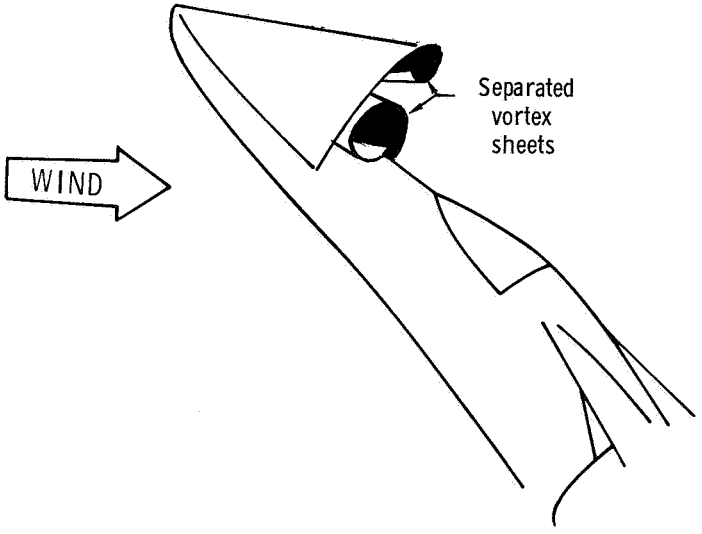

(b) High angles of attack.

Figure 3.- Sketch of the flow phenomena. Asymmetries are indicated at high angles of attack.

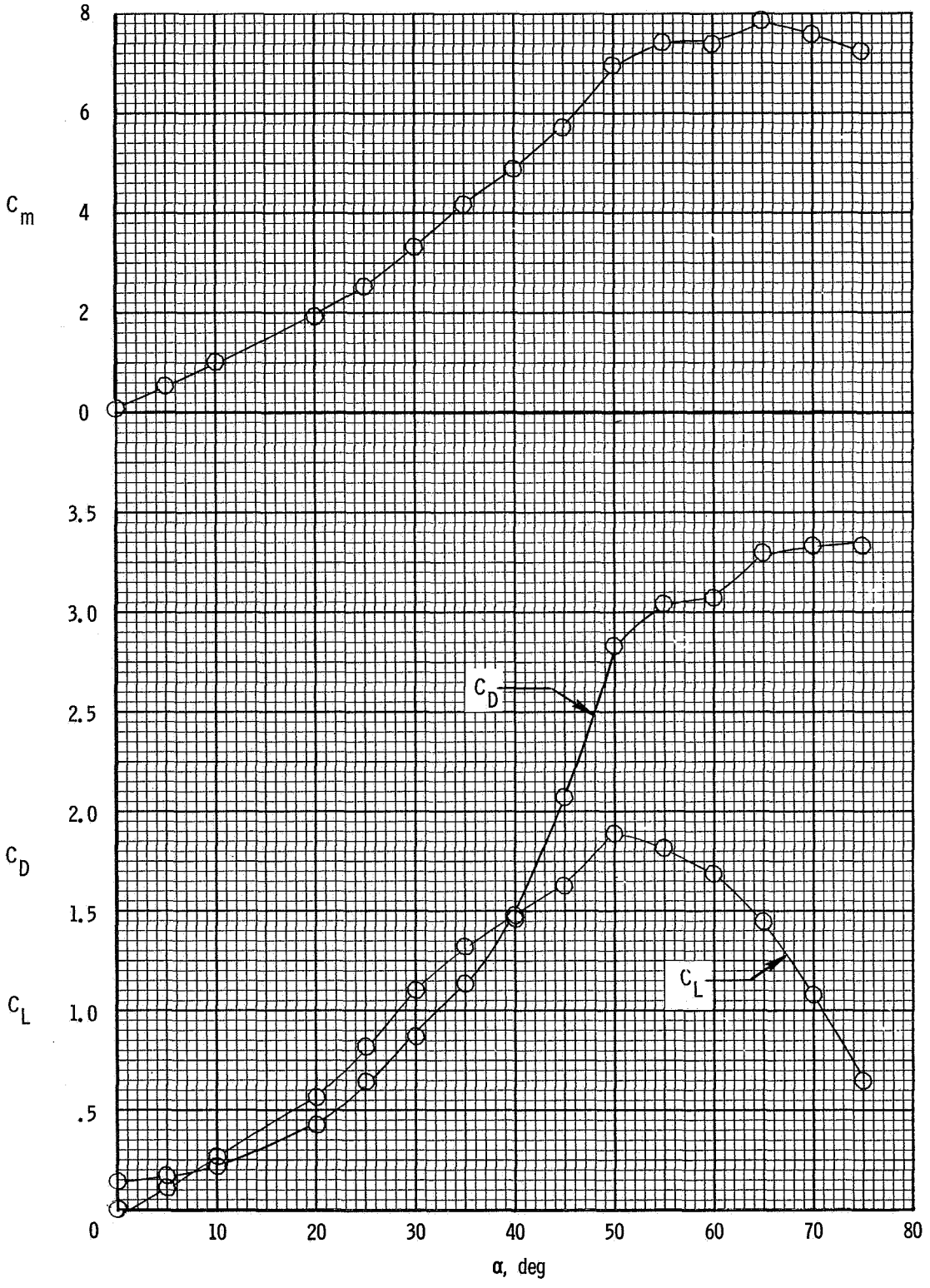

Figure 4.- Longitudinal aerodynamic characteristics of the tangent-ogive model. $\beta = 0^{o}$; $R = 0.35 \times 10^{6}$.

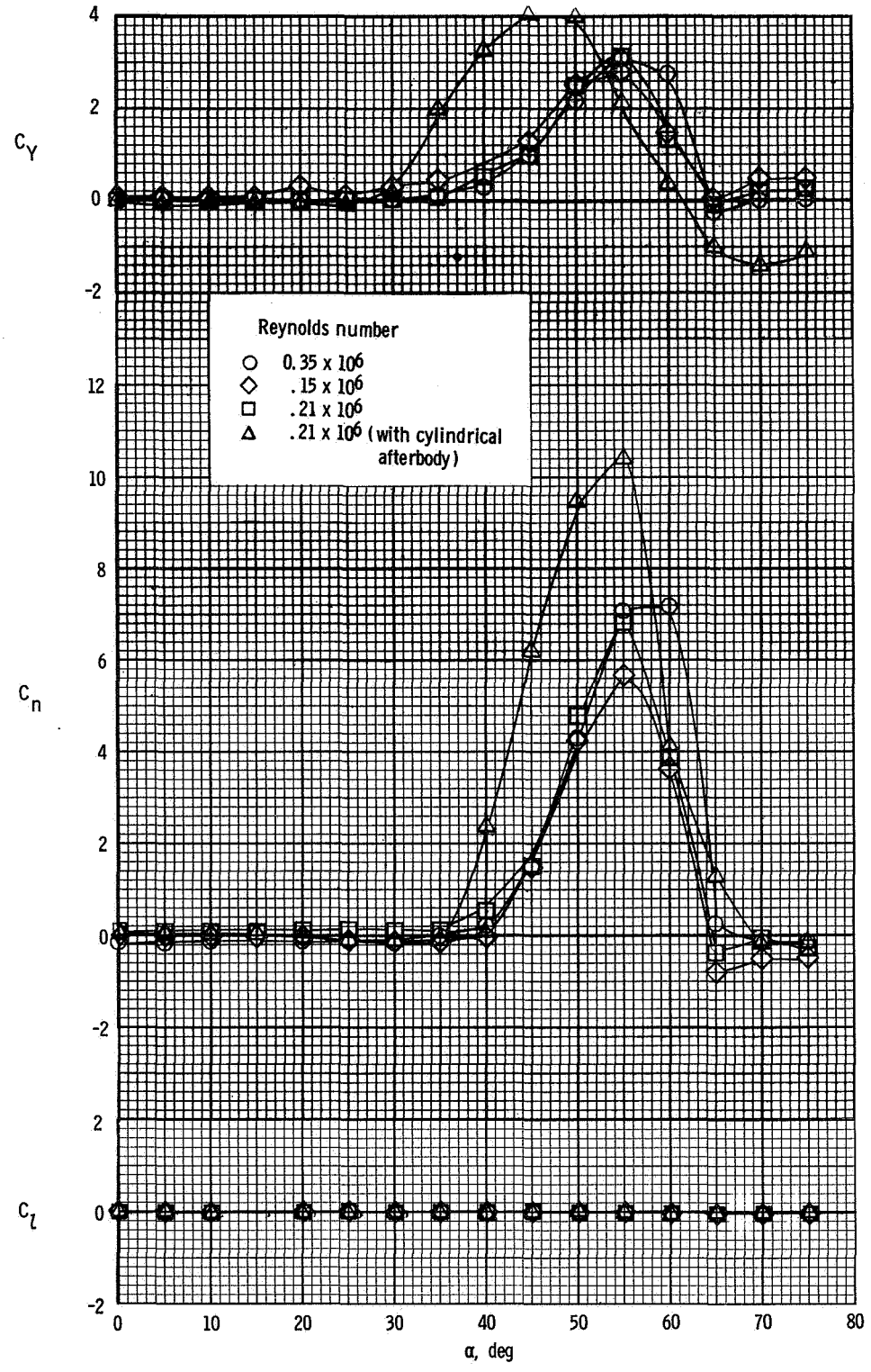

Figure 5.- Lateral-directional aerodynamic characteristics of the tangent-ogive model. $\beta = 0^{o}$.

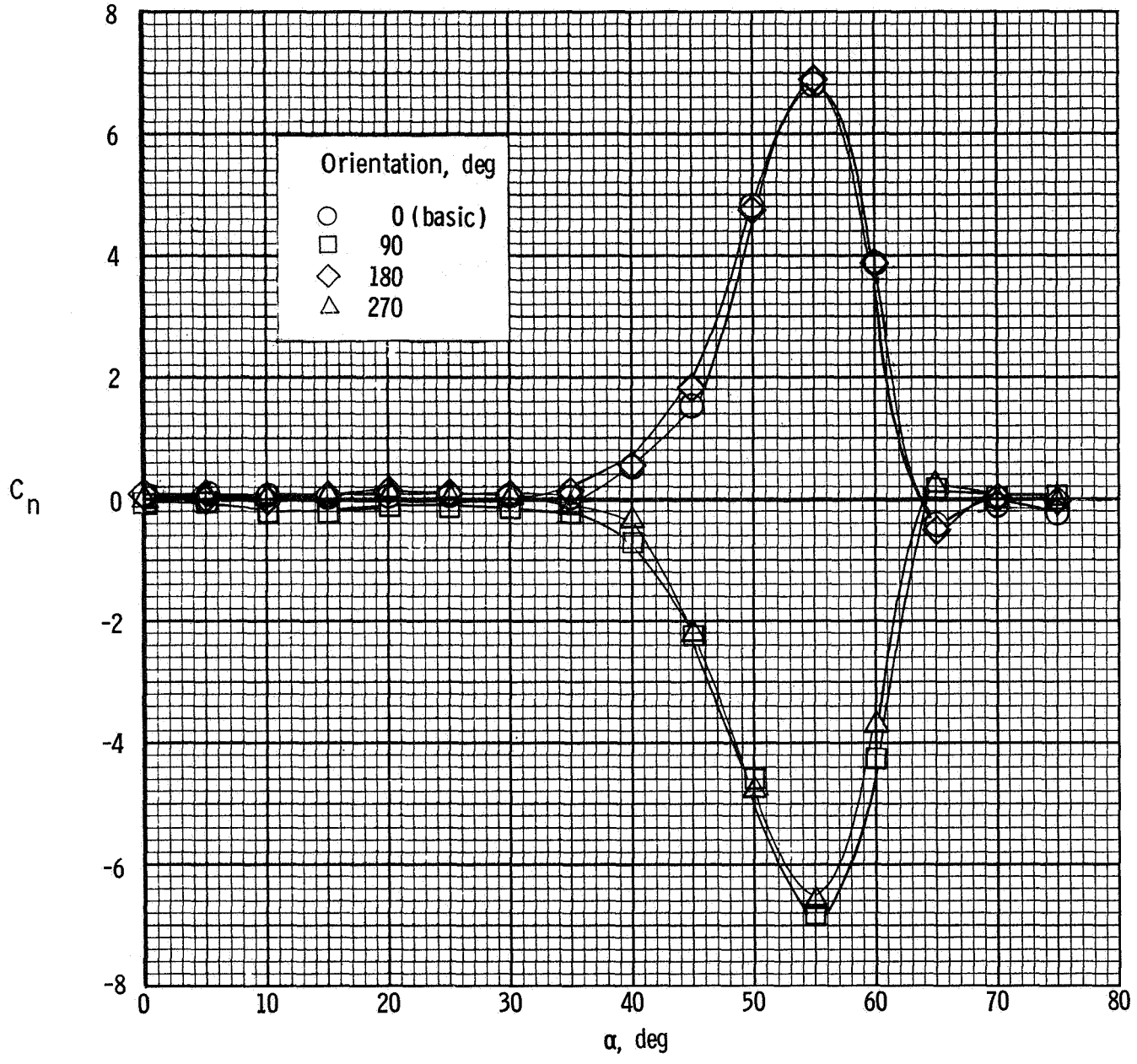

Figure 6.- Effect of reorientation of the tangent-ogive model about the longitudinal axis. $\beta = 0^{o}$; $R = 0.21 \times 10^{6}$.

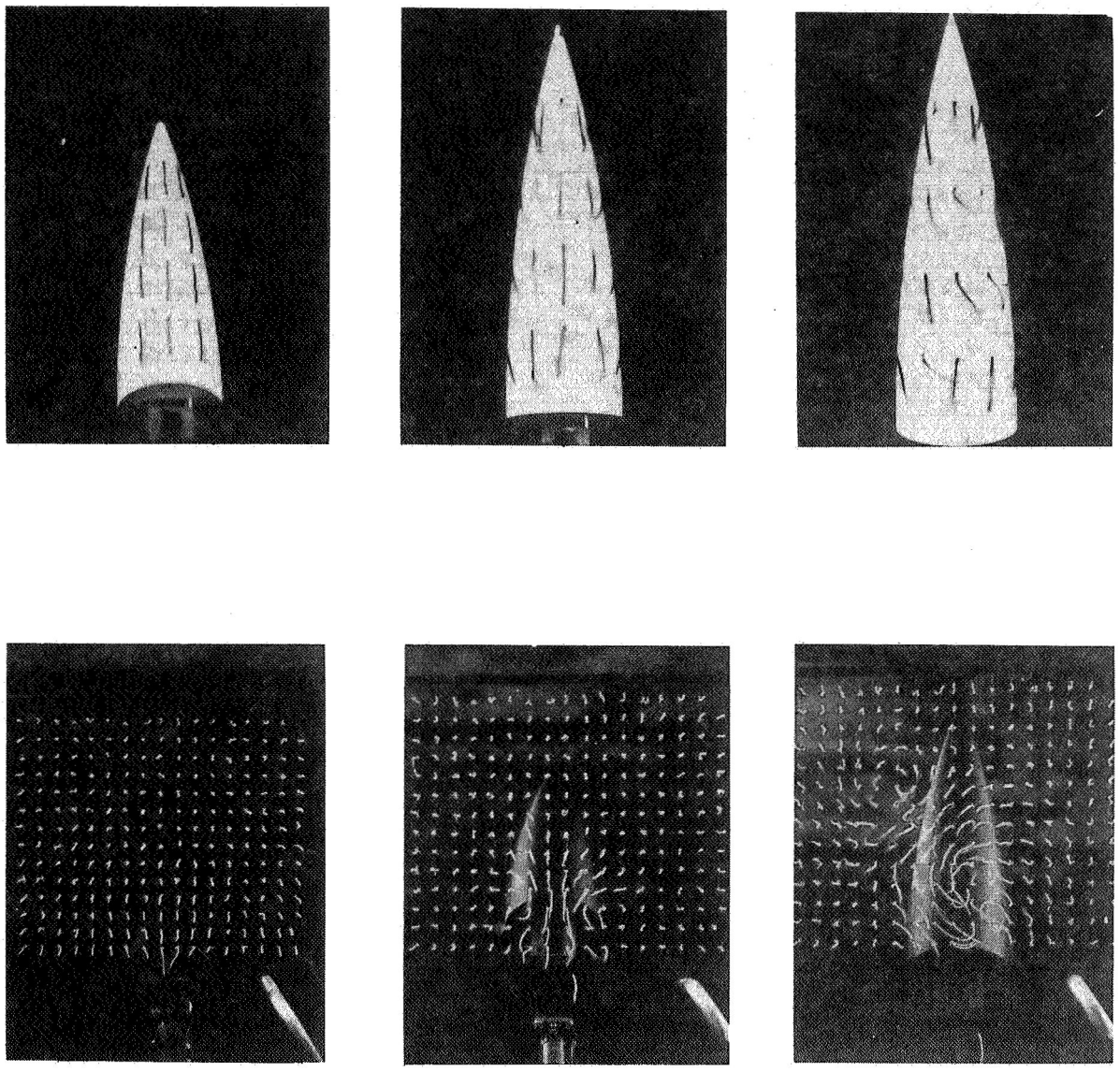

Figure 7.- Results of tuft flow-visualization tests for tangent-ogive model. $\beta = 0^{o}$.

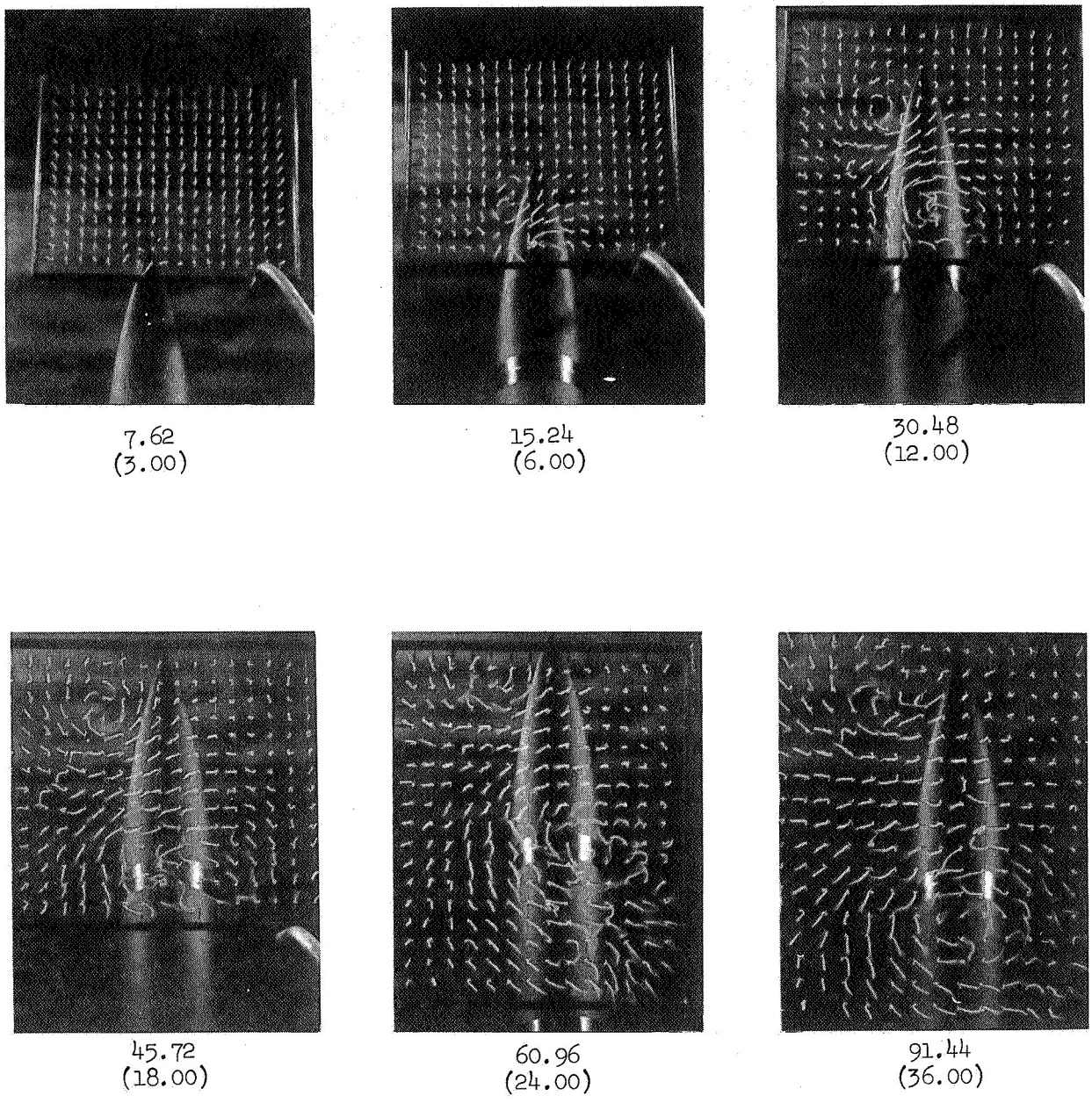

Figure 8.- Tuft grid survey at stations downstream from the nose of the tangent-ogive model with a cylindrical afterbody. $\alpha = 55^{o}$; $\beta = 0^{o}$. Dimensions are given in centimeters (inches).

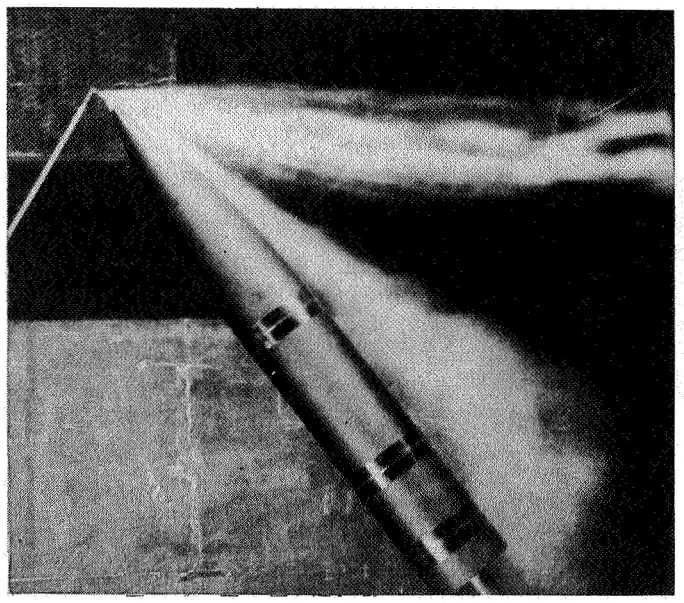

(a) Tangent-ogive model with cylindrical afterbody.

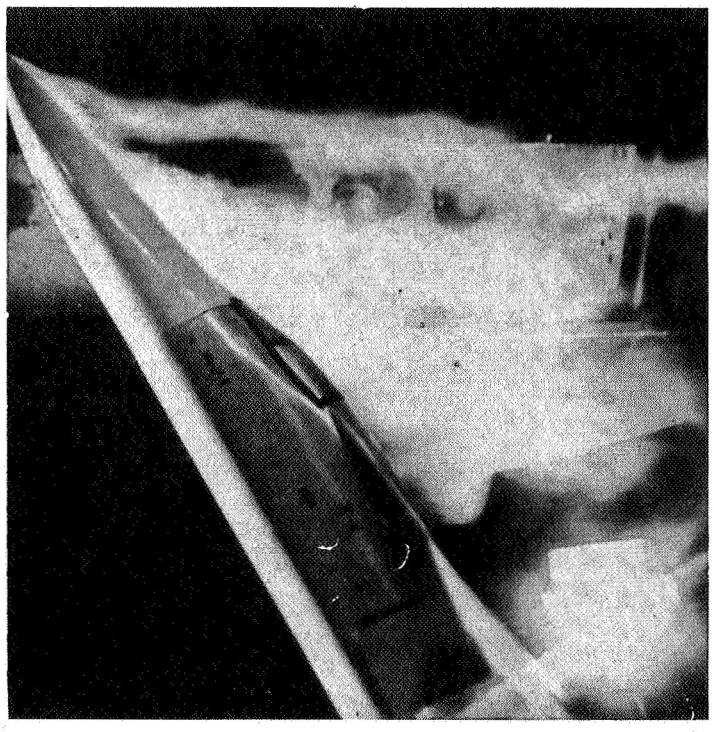

(b) Model of reference 1.

Figure 9.- Comparison of smoke flow-visualization results of present investigation with those of reference 1.

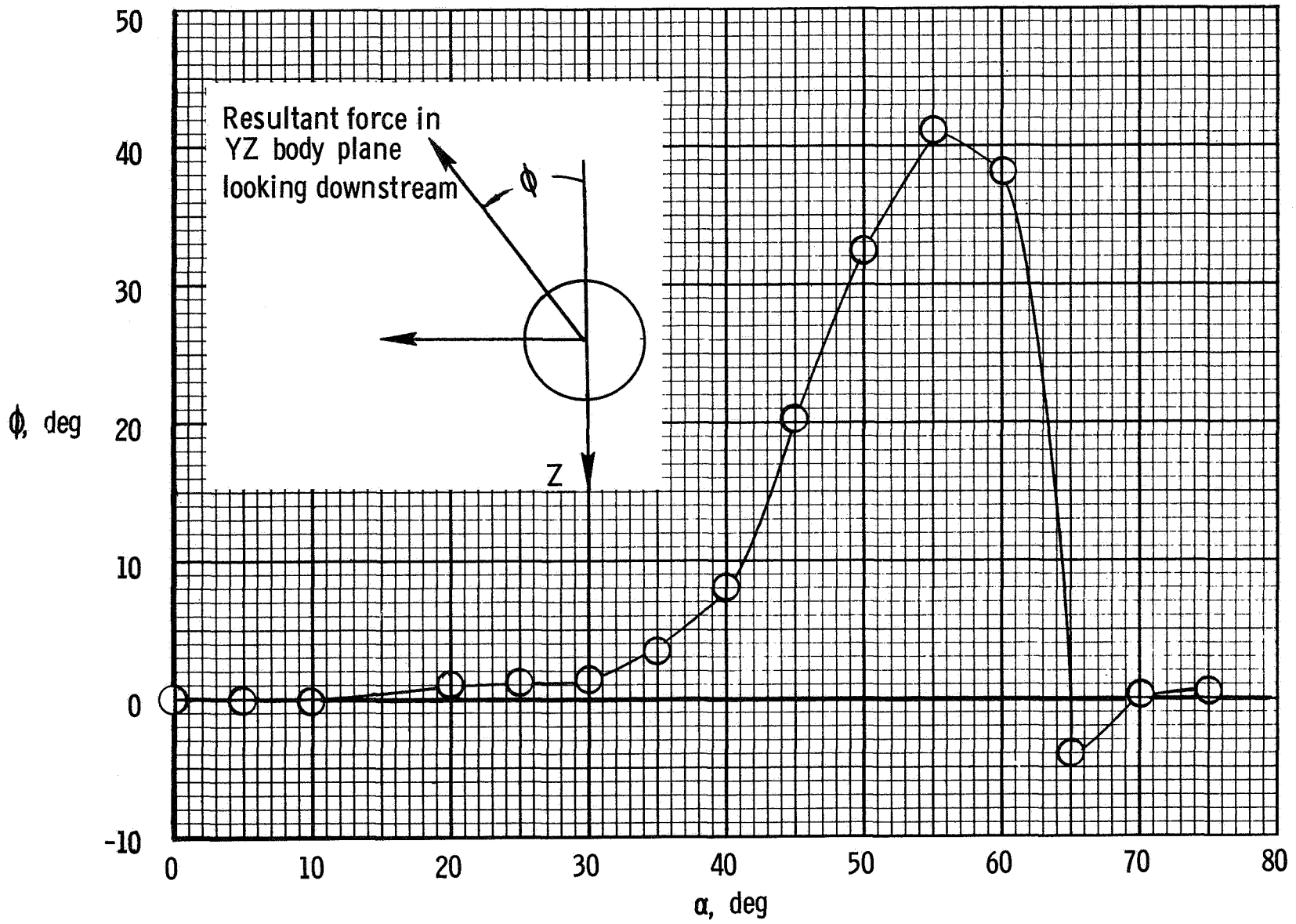

Figure 10.- Inclination of the resultant force acting in the YZ body plane of the tangent-ogive model. $\beta = 0^{o}$; $R = 0.35 \times 10^{6}$.

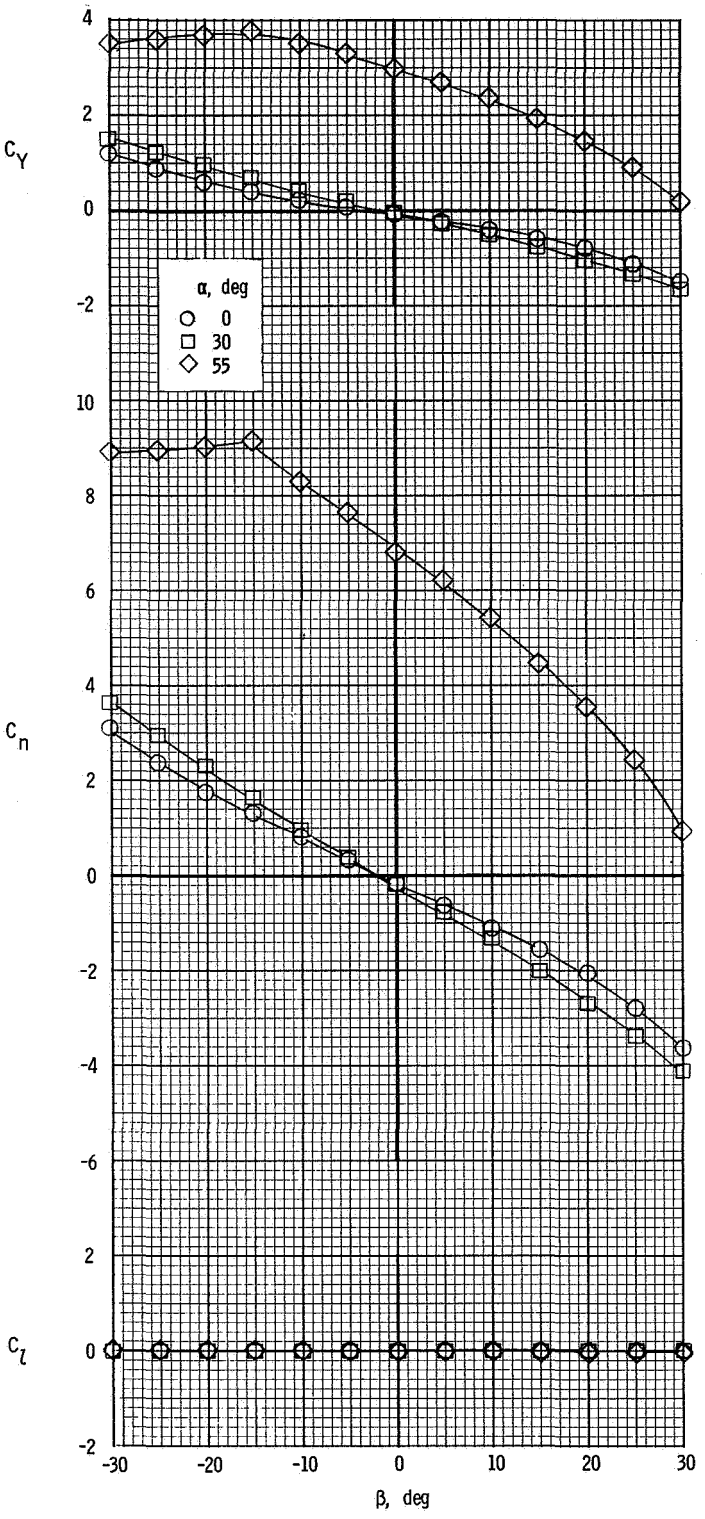

Figure 11.- Effect of sideslip angle on the characteristics of the tangent-ogive model. $R = 0.35 \times 10^6$.

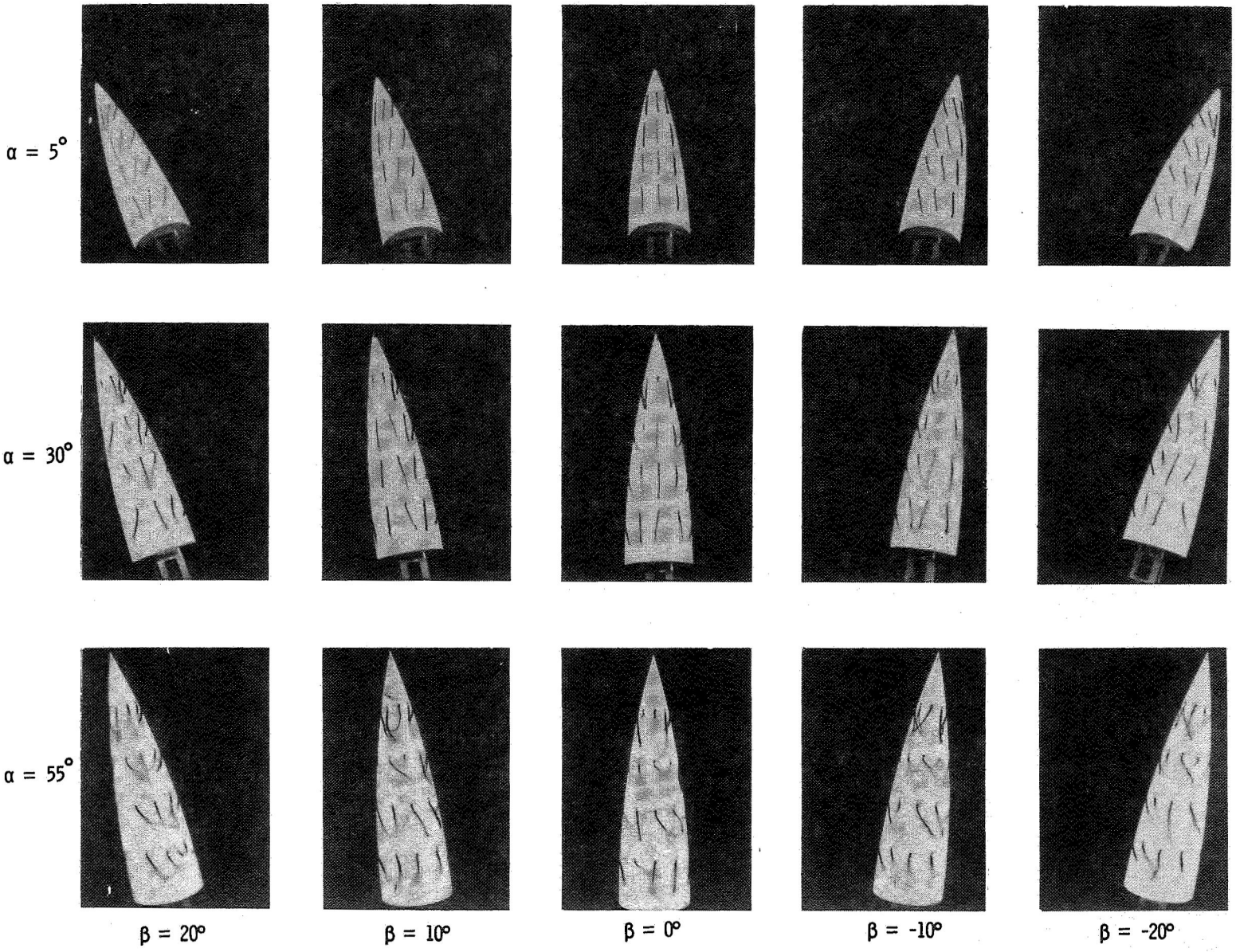

(a) Tufts on surface.

Figure 12.- Flow-visualization photographs of the effect of sideslip for the tangent-ogive model.

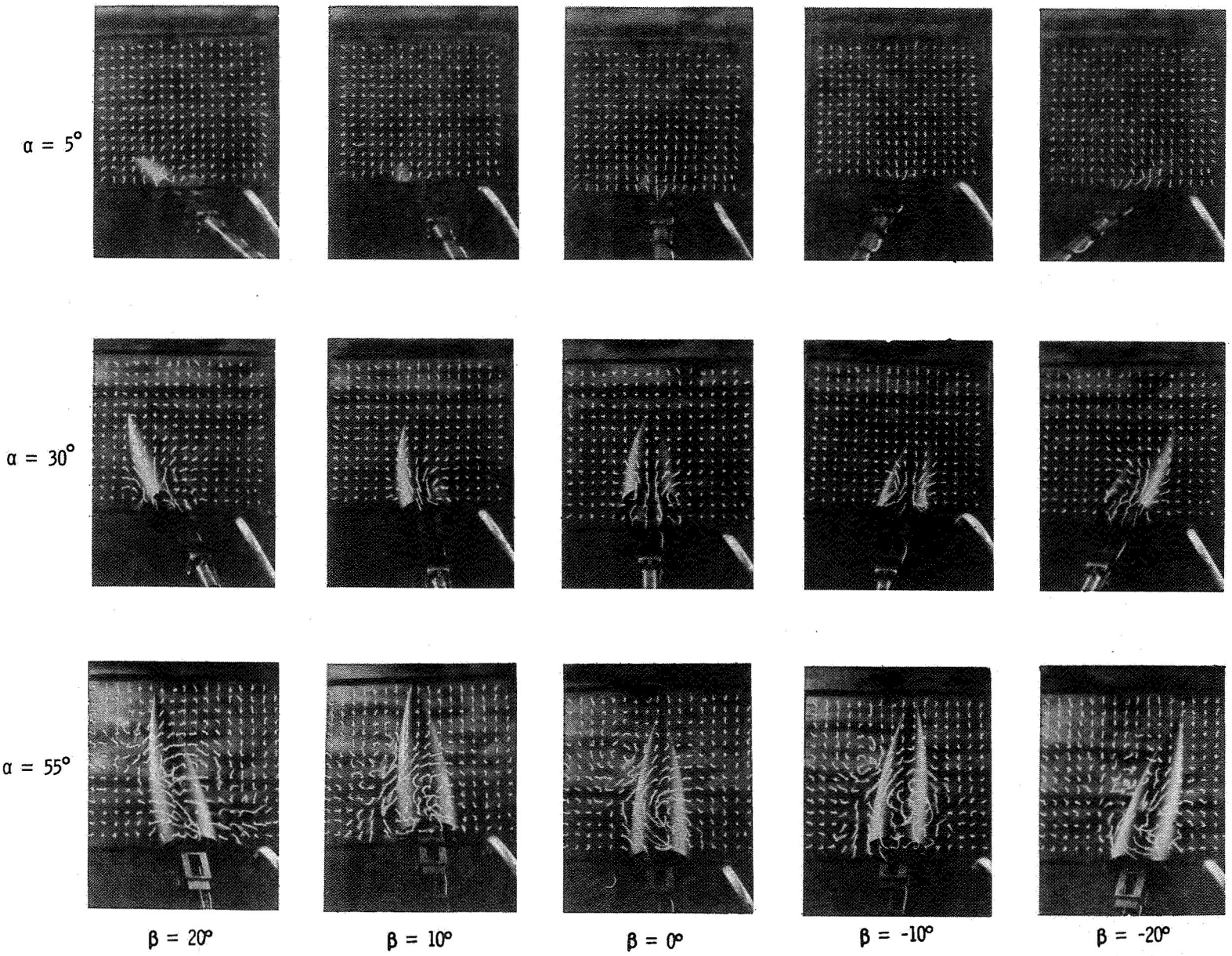

(b) Tuft grid.

Figure 12.- Concluded.

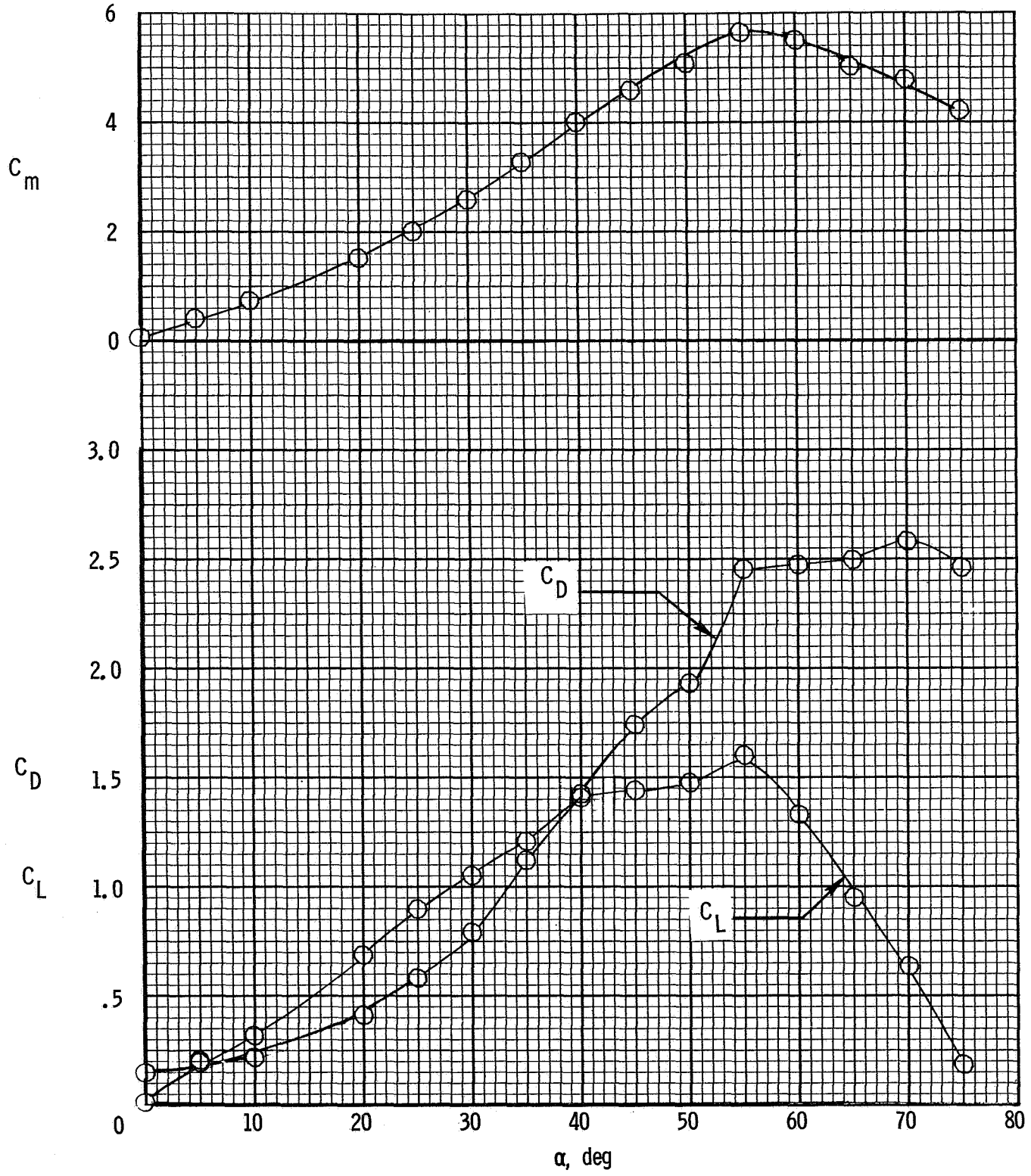

Figure 13.- Longitudinal aerodynamic characteristics of the cone.
$\beta = 0^o$; $R = 0.35 \times 10^6$.

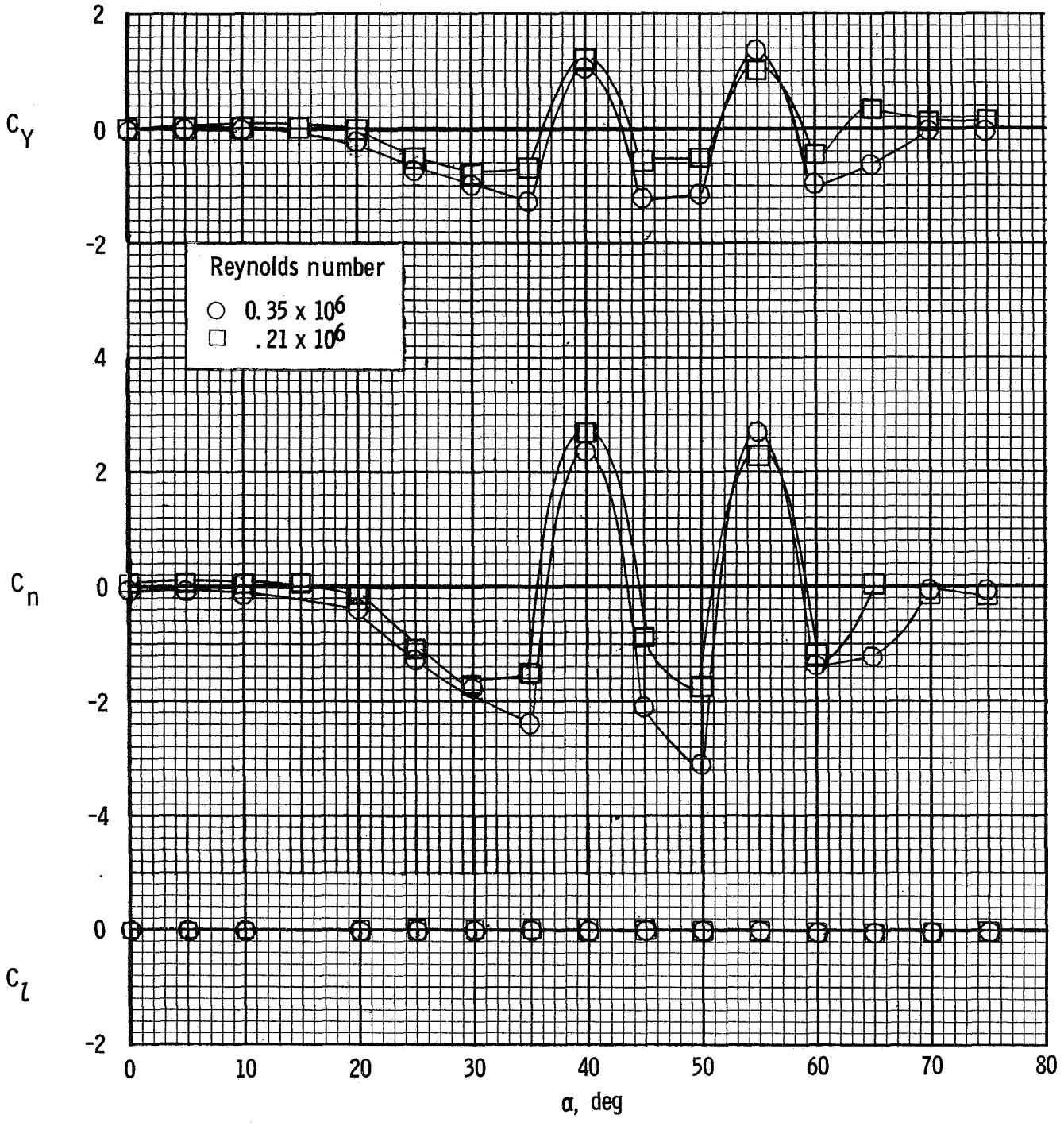

(a) 0^o orientation.

Figure 14.- Lateral-directional aerodynamic characteristics of the cone. $\beta = 0^o$.

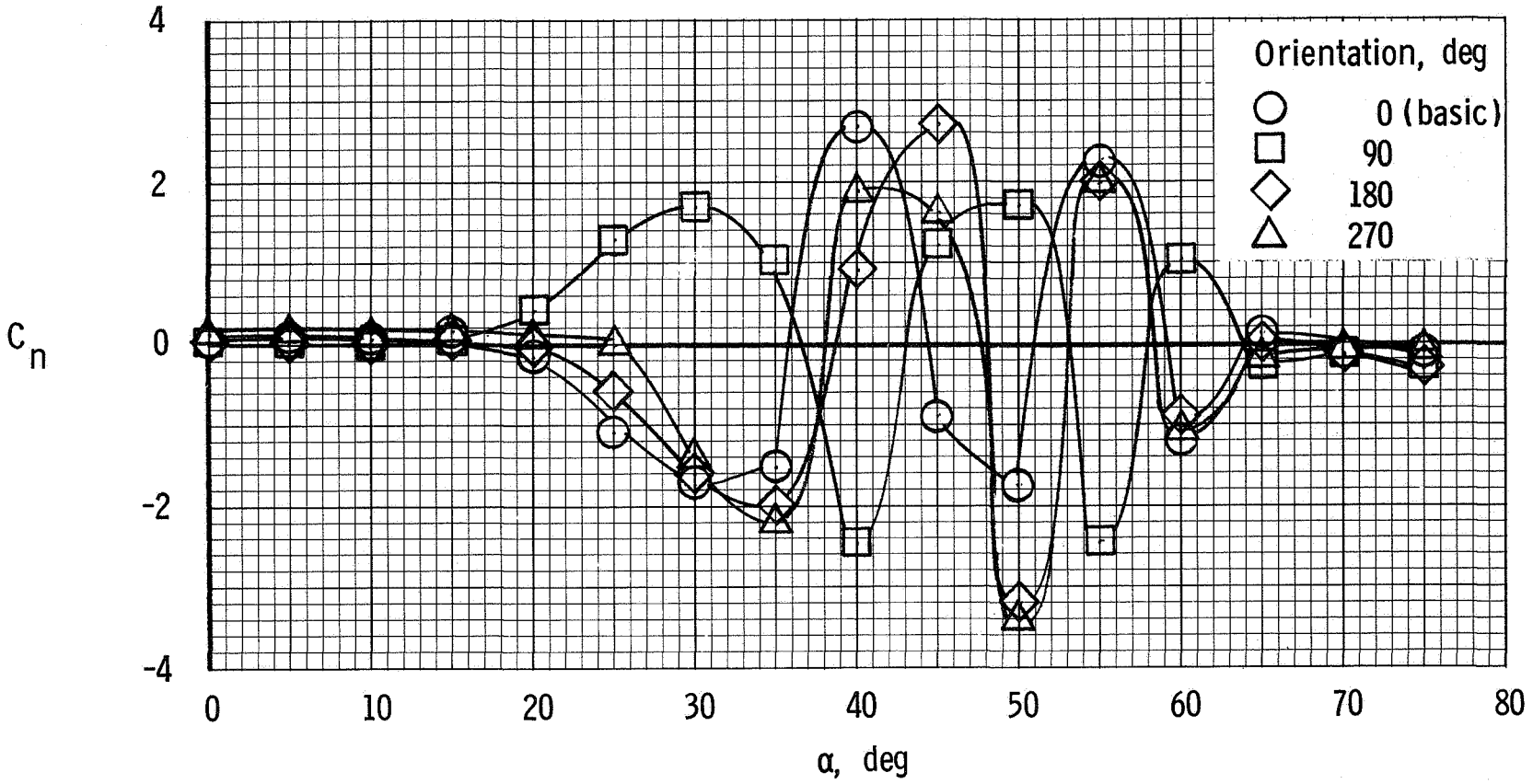

(b) Effect of reorientation of the cone about the longitudinal axis. $\beta = 0^{o}$; $R = 0.21 \times 10^{6}$.

Figure 14.- Concluded.

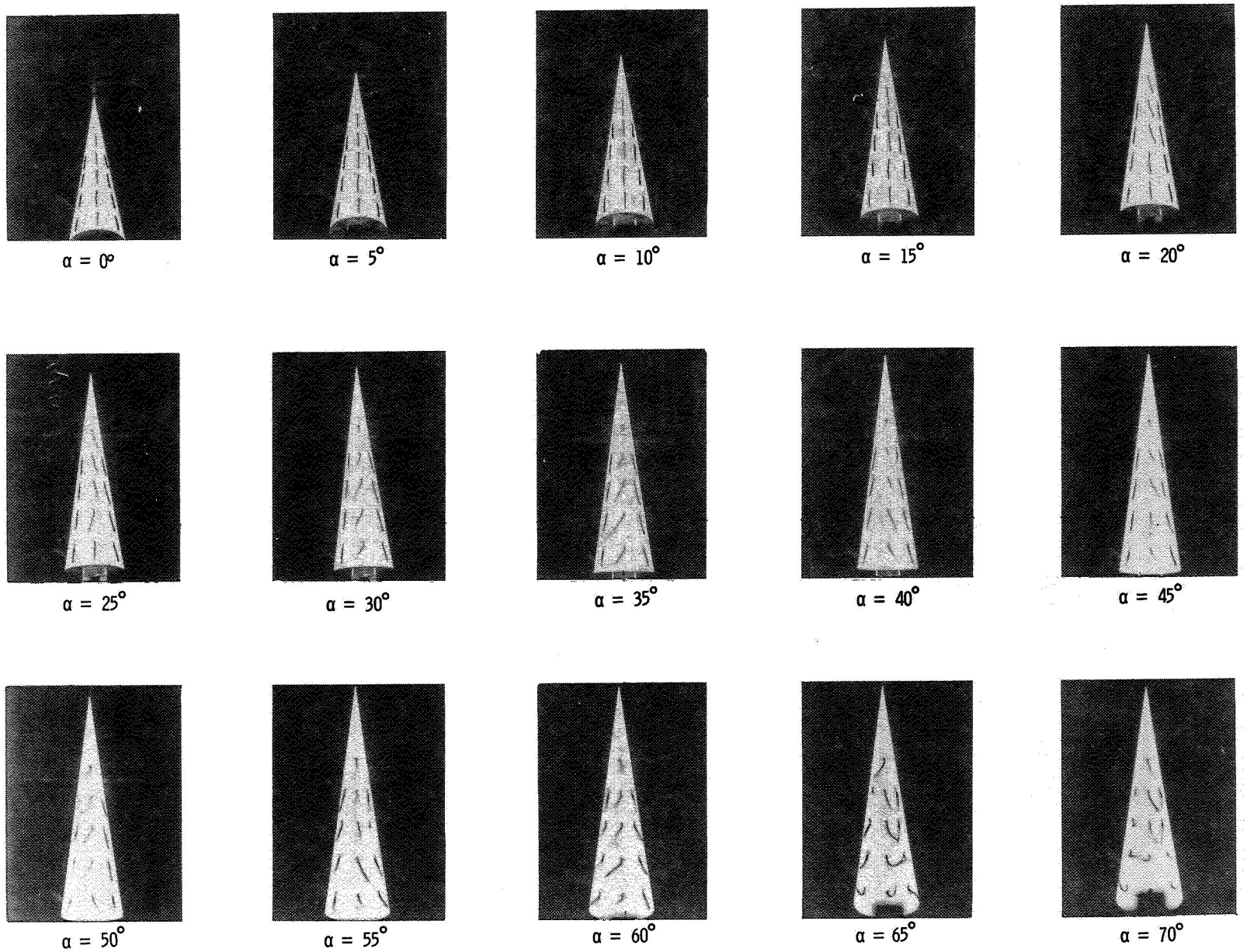

(a) Tufts on surface.

Figure 15.- Flow-visualization photographs for the cone. $\beta = 0^{o}$.

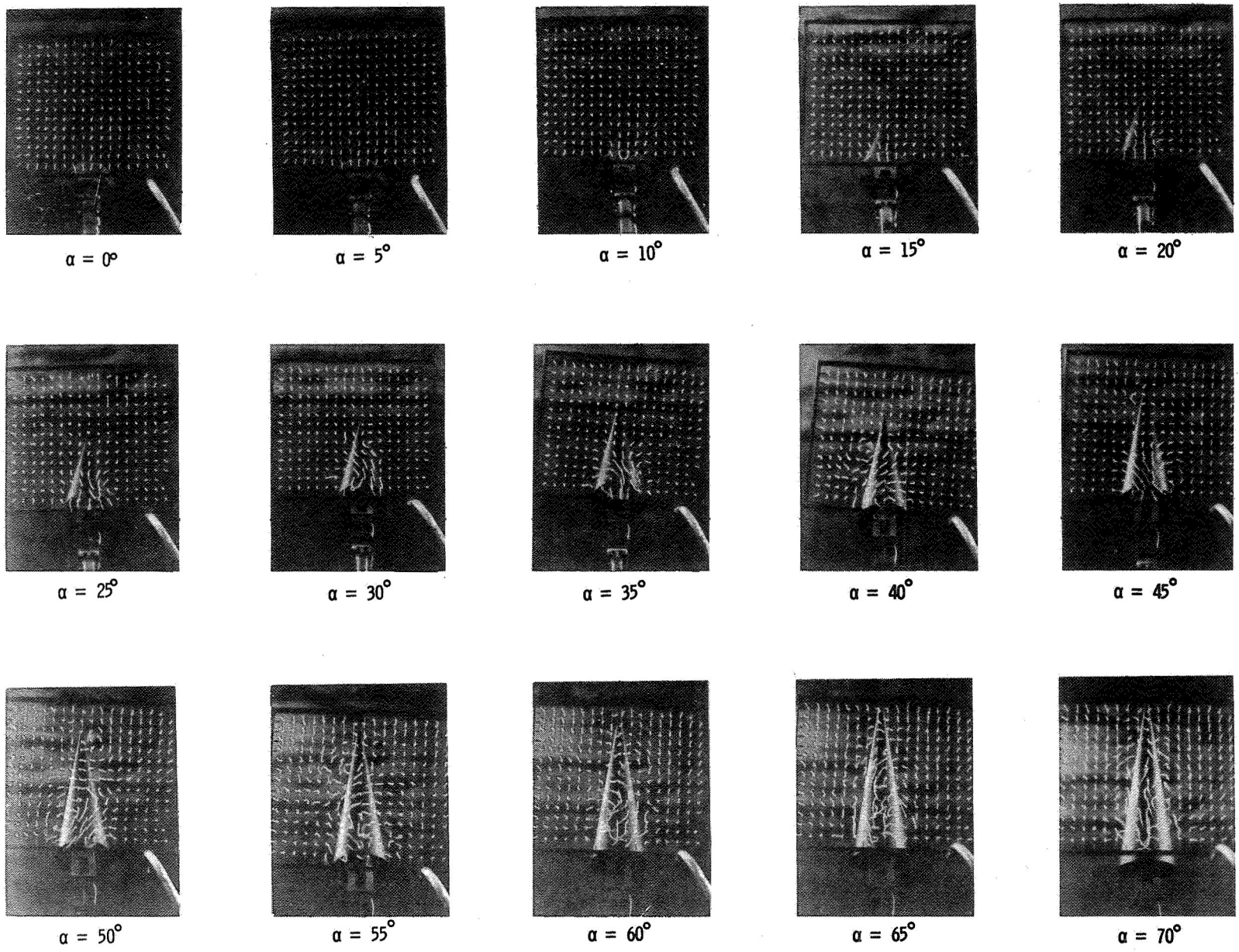

(b) Tuft grid.

Figure 15.- Concluded.

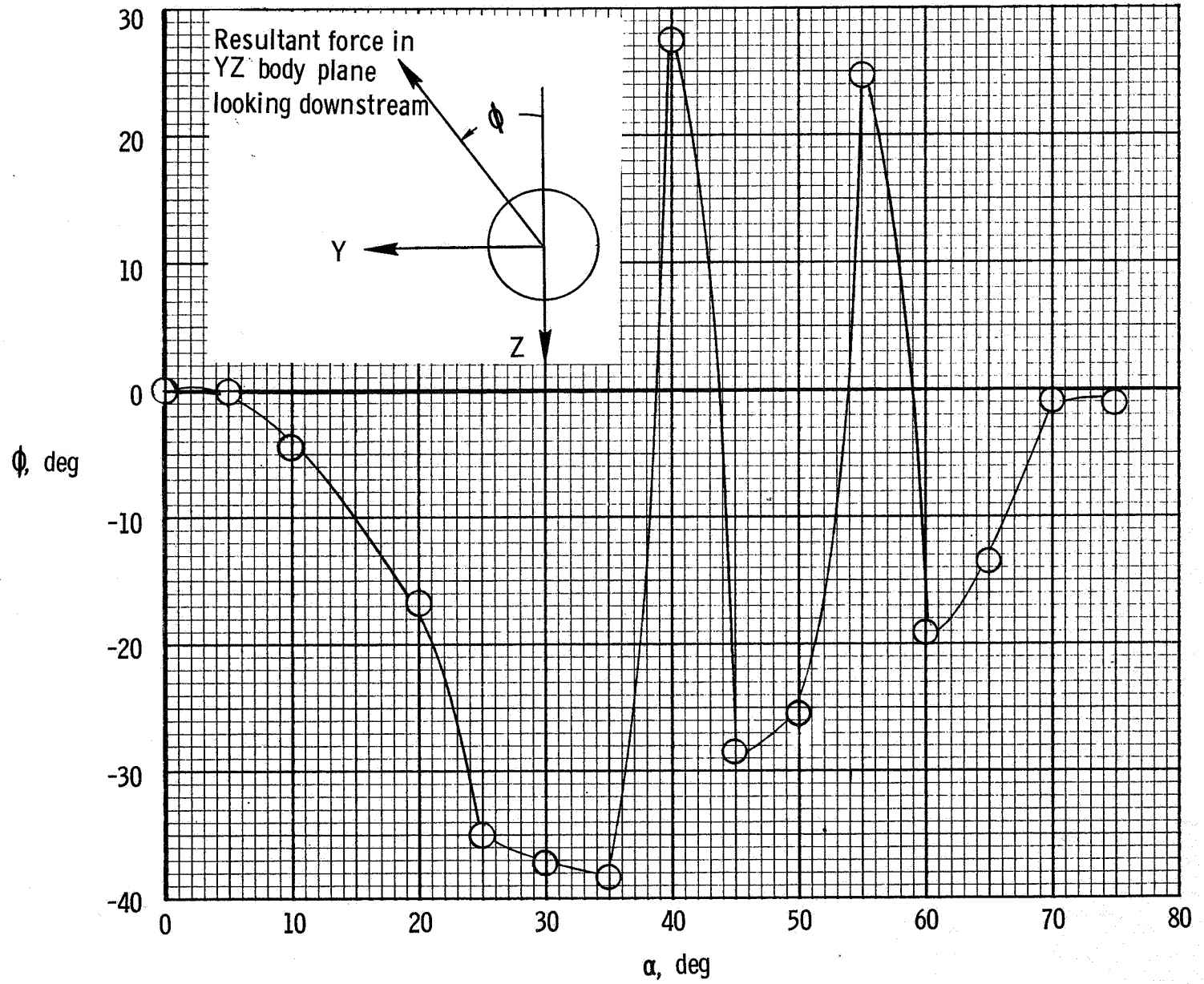

Figure 16.- Inclination of the resultant force acting in the YZ body plane of the cone. $\beta = 0^{o}$; $R = 0.35 \times 10^{6}$.

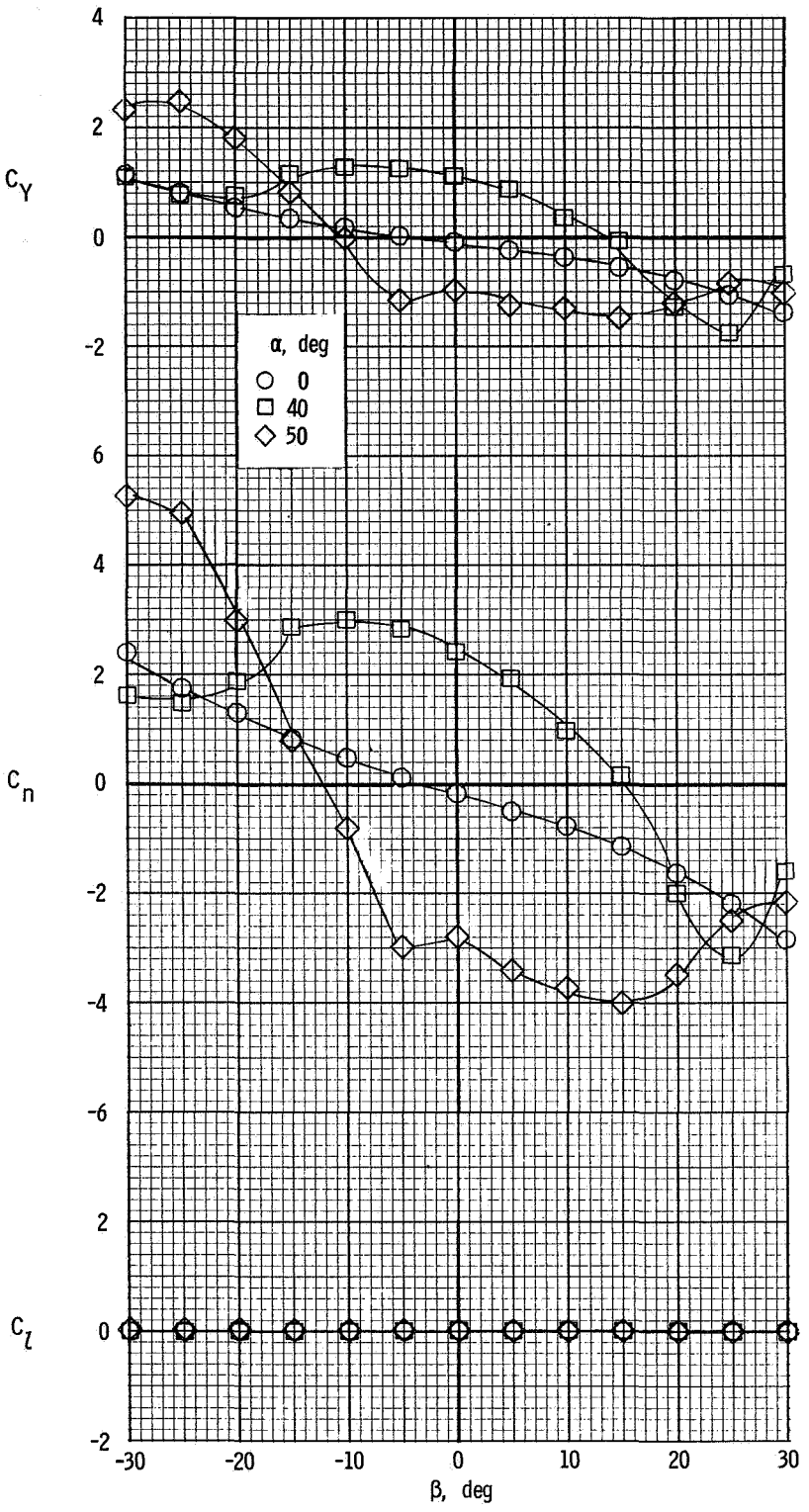

Figure 17.- Effect of sideslip angle on characteristics of the cone. $R = 0.35 \times 10^6$.

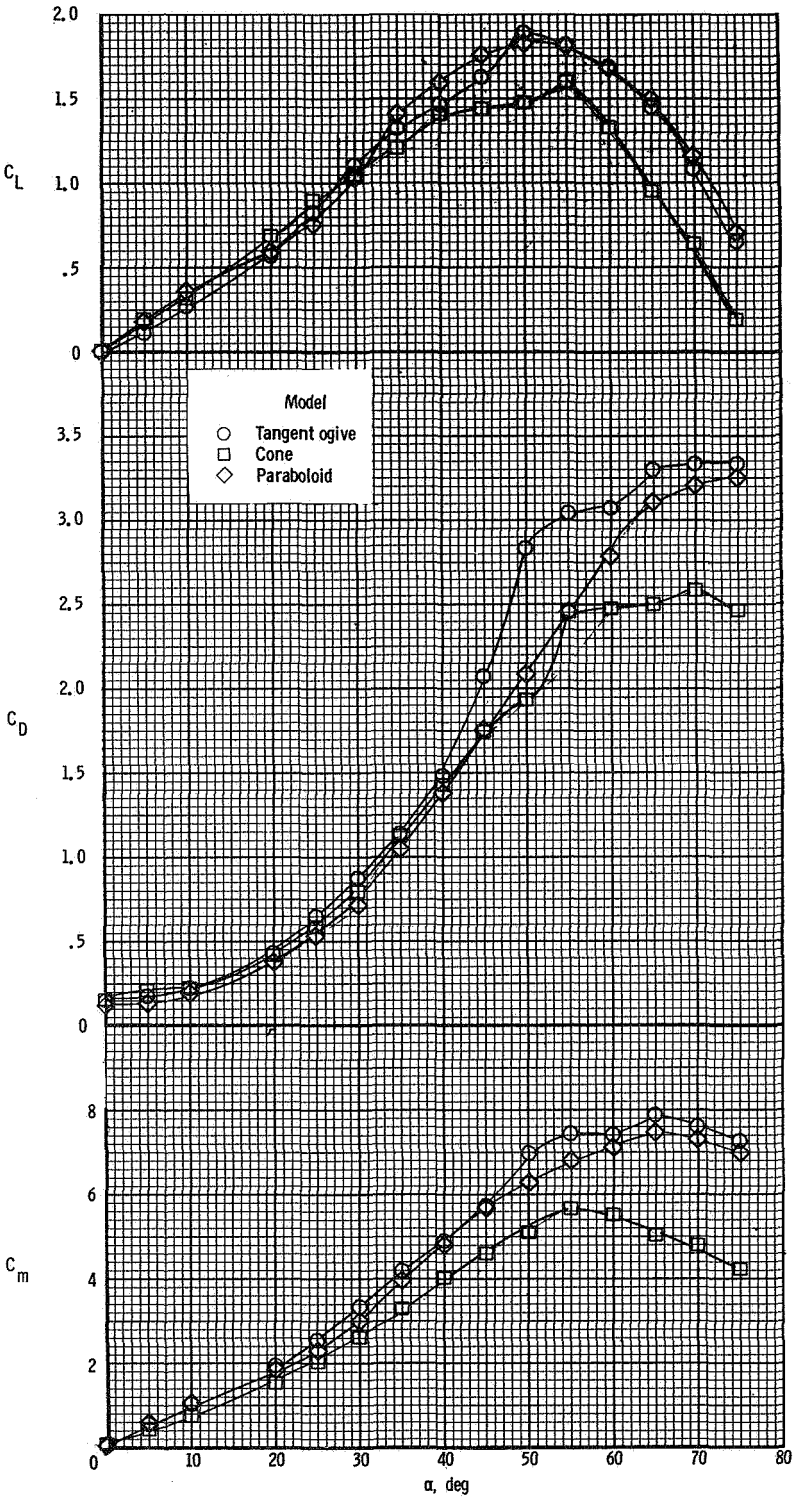

Figure 18.- Comparison of longitudinal characteristics of the tangent-ogive model, cone, and paraboloid. $\beta = 0^o$; $R = 0.35 \times 10^6$.

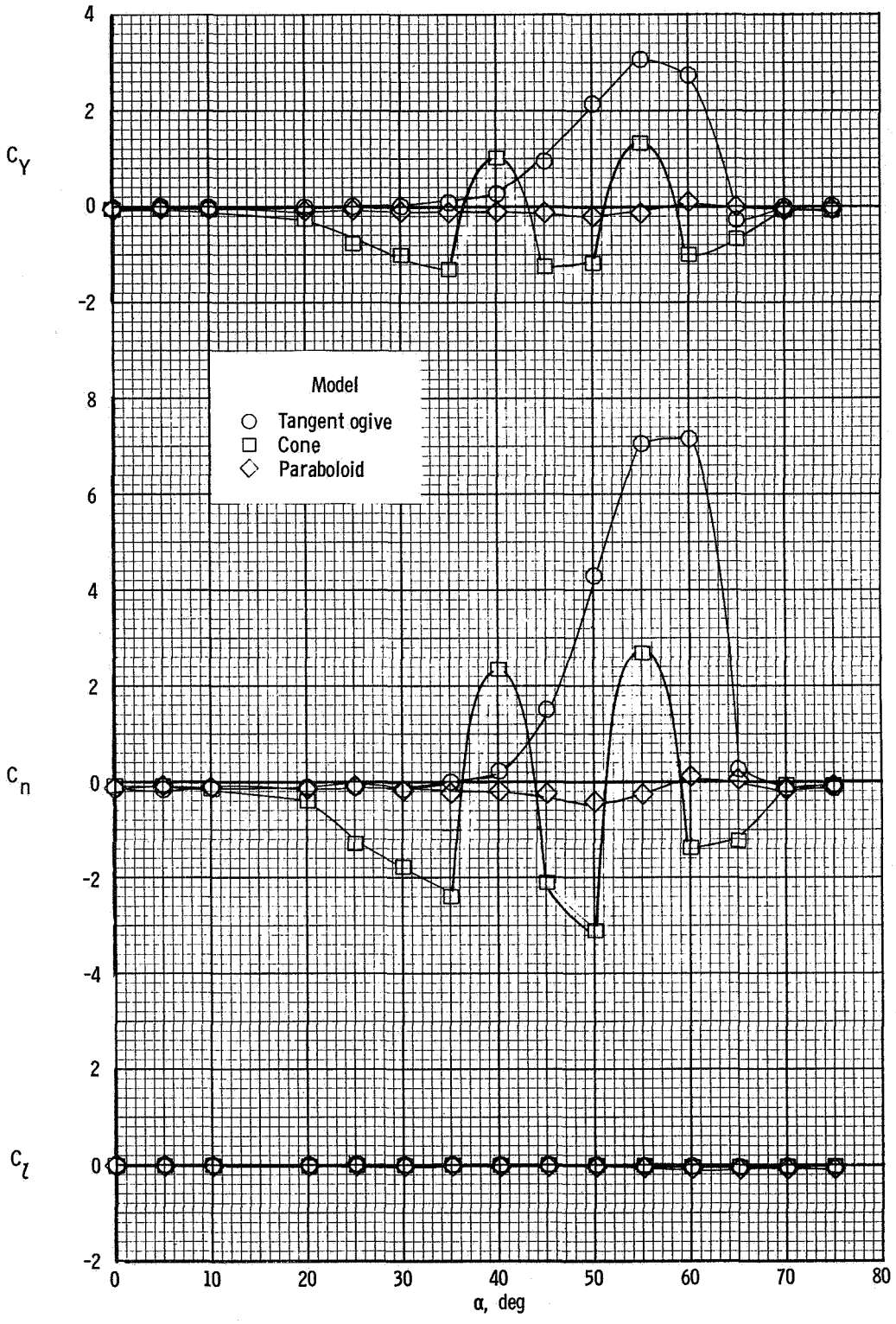

Figure 19.- Comparison of the lateral-directional aerodynamic characteristics of the tangent-ogive model, cone, and paraboloid. $\beta = 0^{o}$; $R = 0.35 \times 10^{6}$.

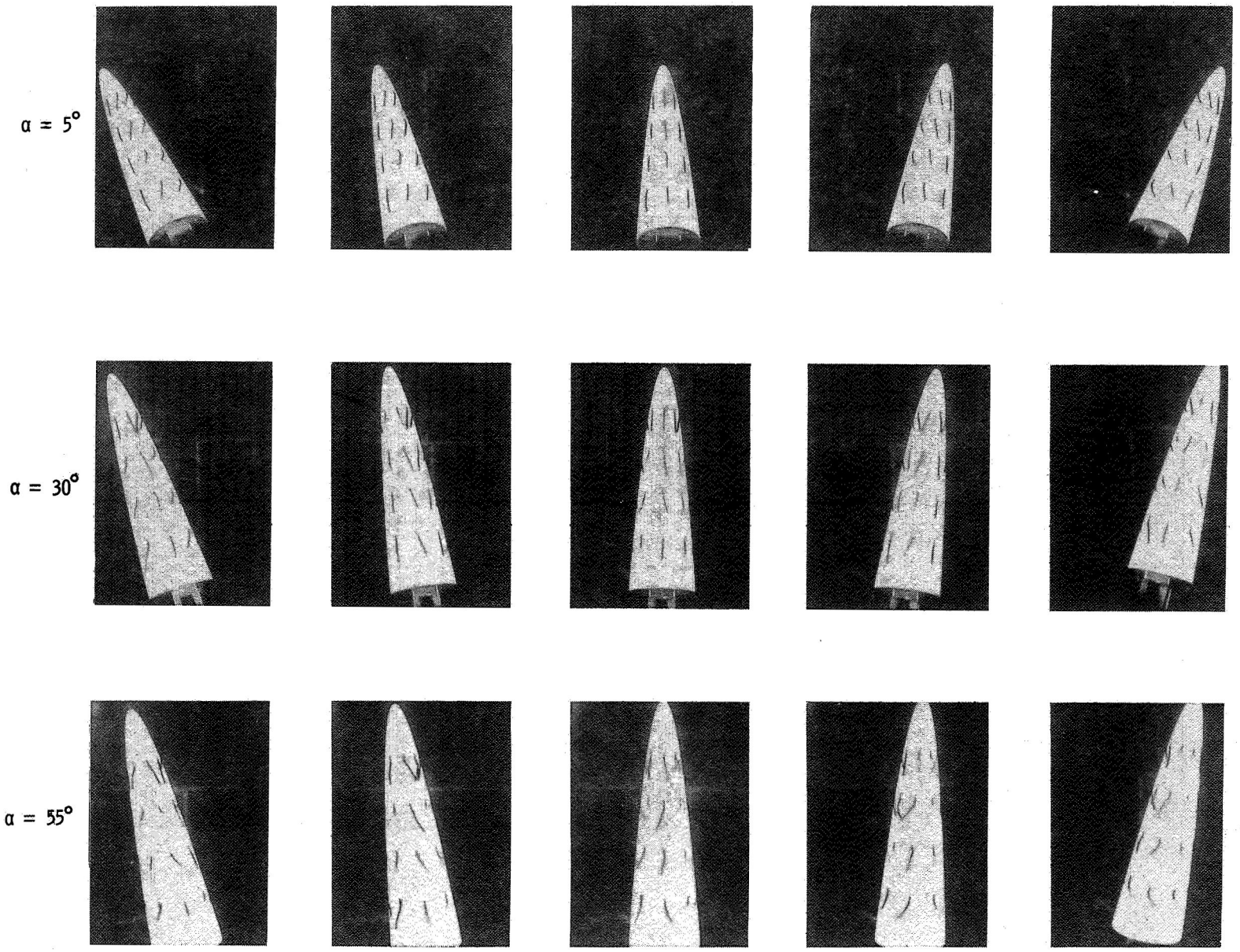

Figure 20.- Surface tuft photograph for the paraboloid of revolution.

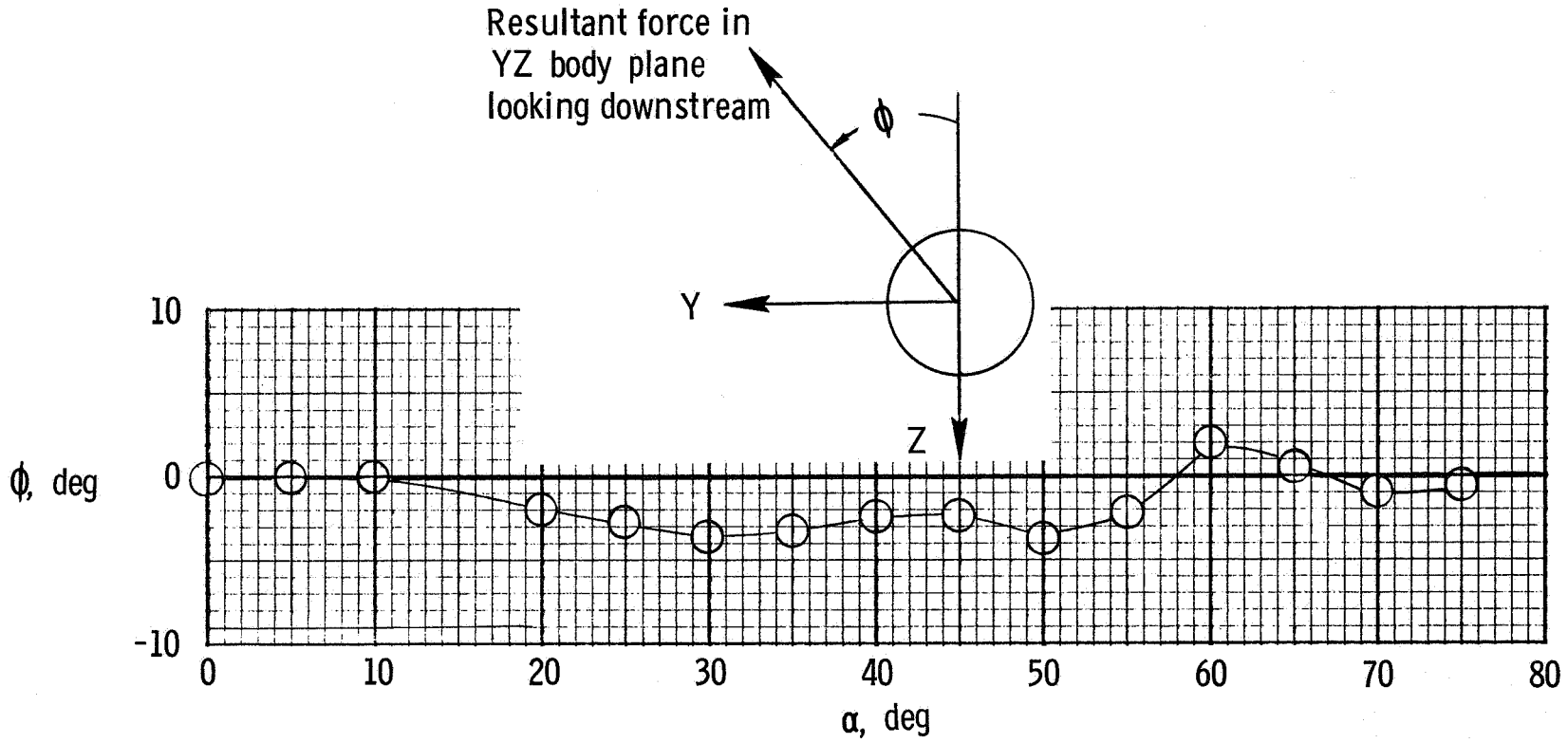

Figure 21.- Inclination of the resultant force acting in the YZ body plane of the paraboloid. $\beta = 0^{o}$; $R = 0.35 \times 10^{6}$.

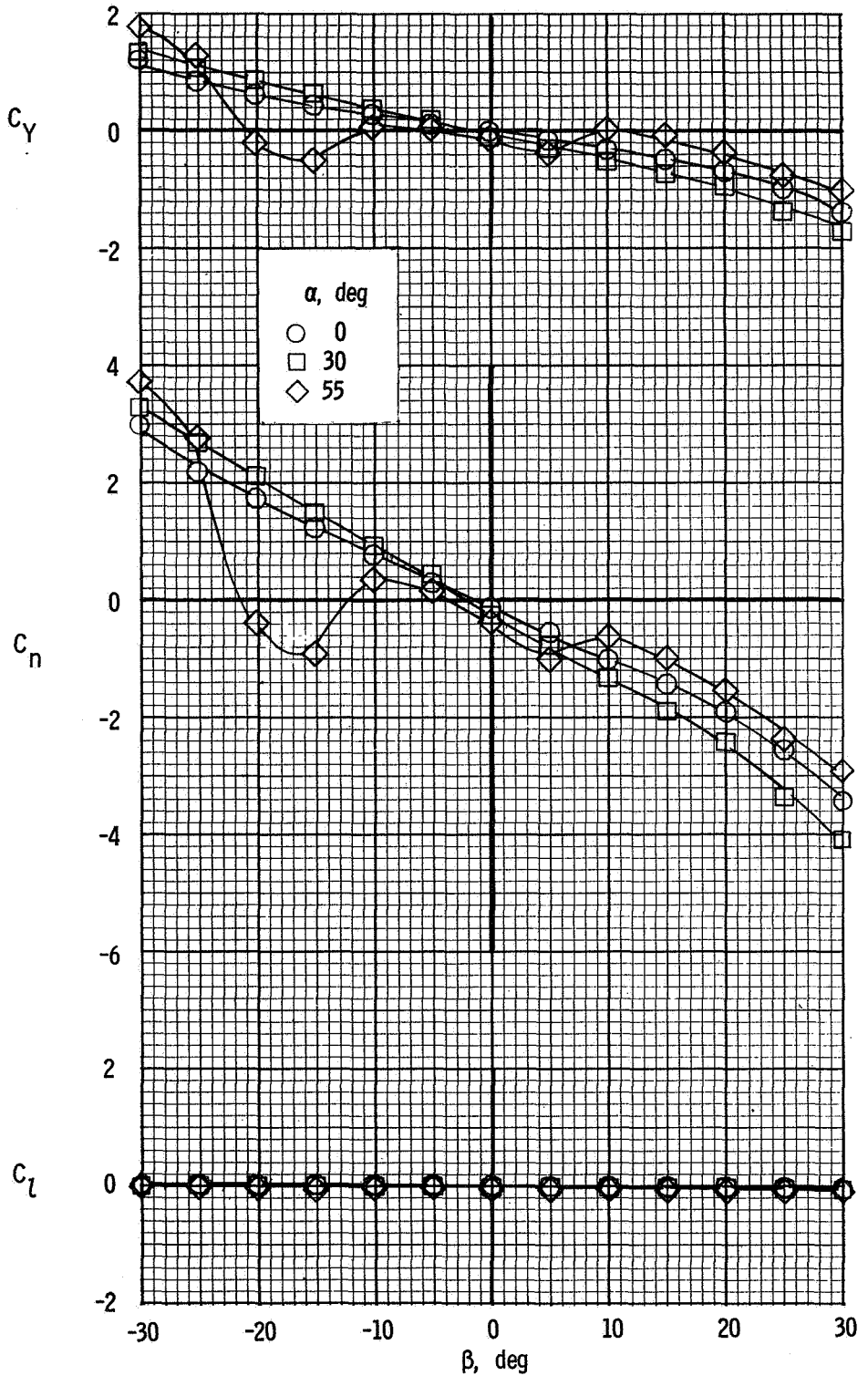

Figure 22.- Effect of sideslip angle on characteristics of the paraboloid.

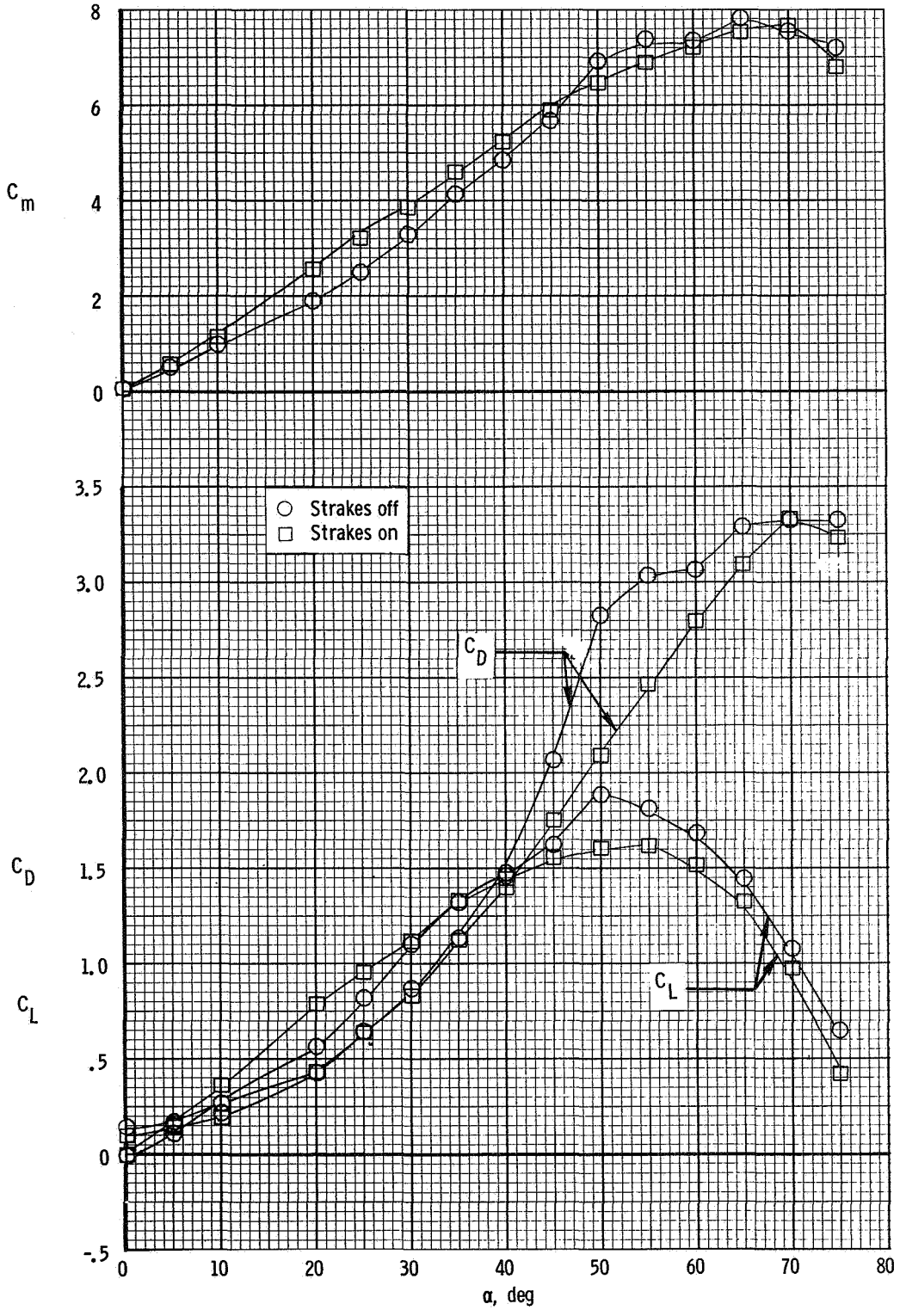

(a) Tangent-ogive model.

Figure 23.- Effect of strakes on the longitudinal aerodynamic characteristics. $\beta = 0^{o}$; $R = 0.35 \times 10^{6}$.

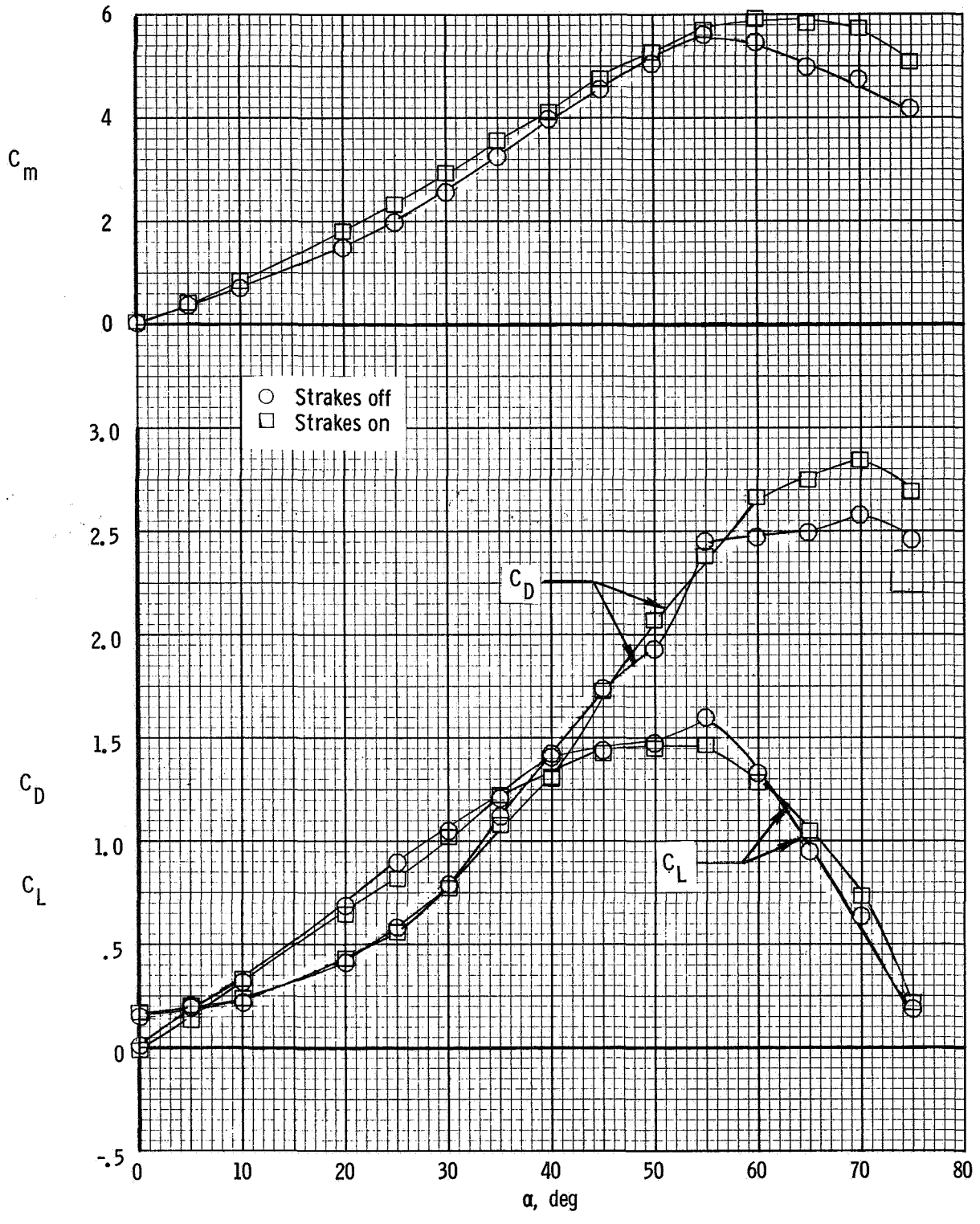

(b) Cone.

Figure 23.- Concluded.

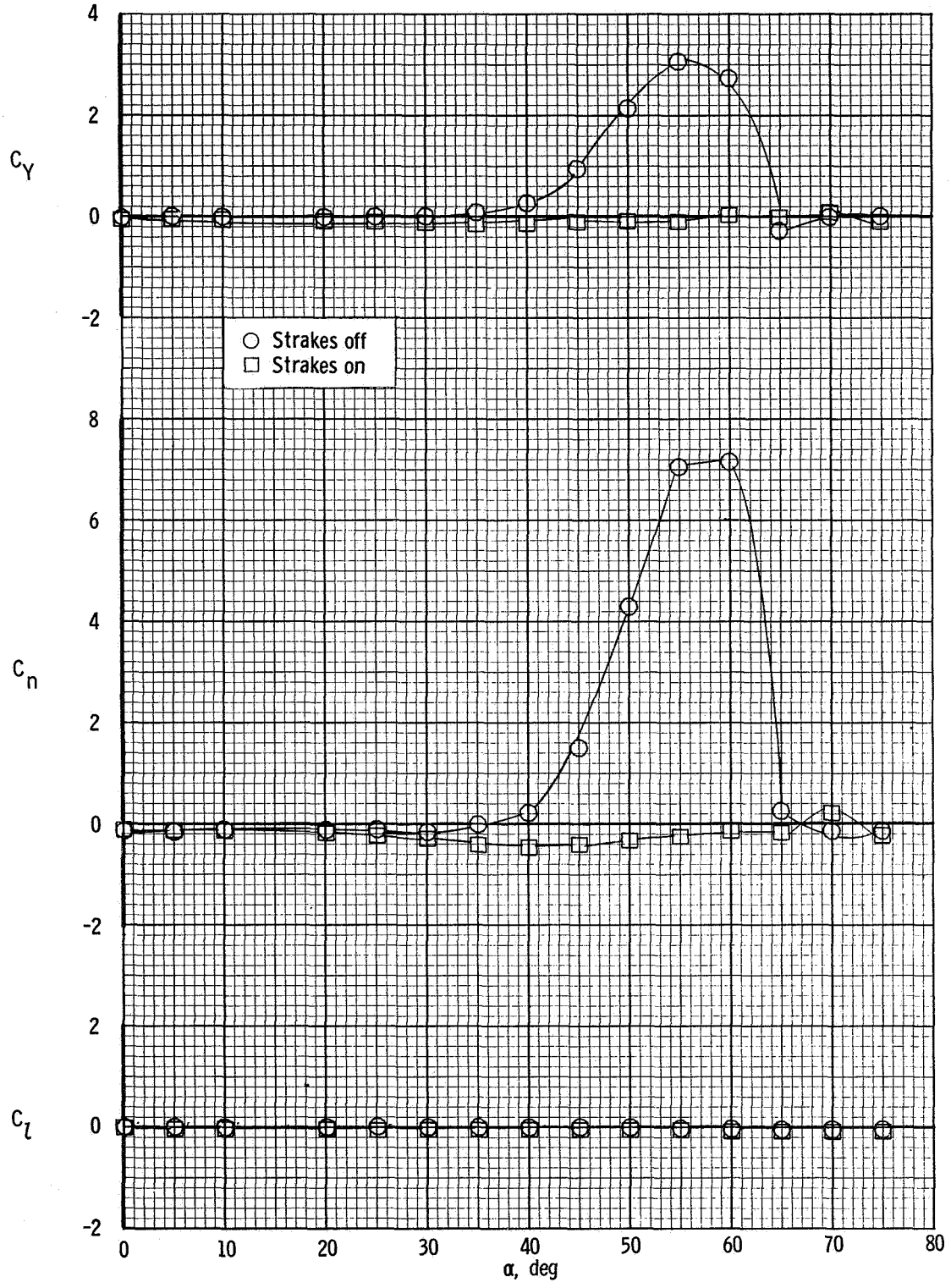

(a) Tangent-ogive model.

Figure 24.- Effect of strakes on the lateral-directional aerodynamic characteristics. $\beta = 0^{o}$; $R = 0.35 \times 10^{6}$.

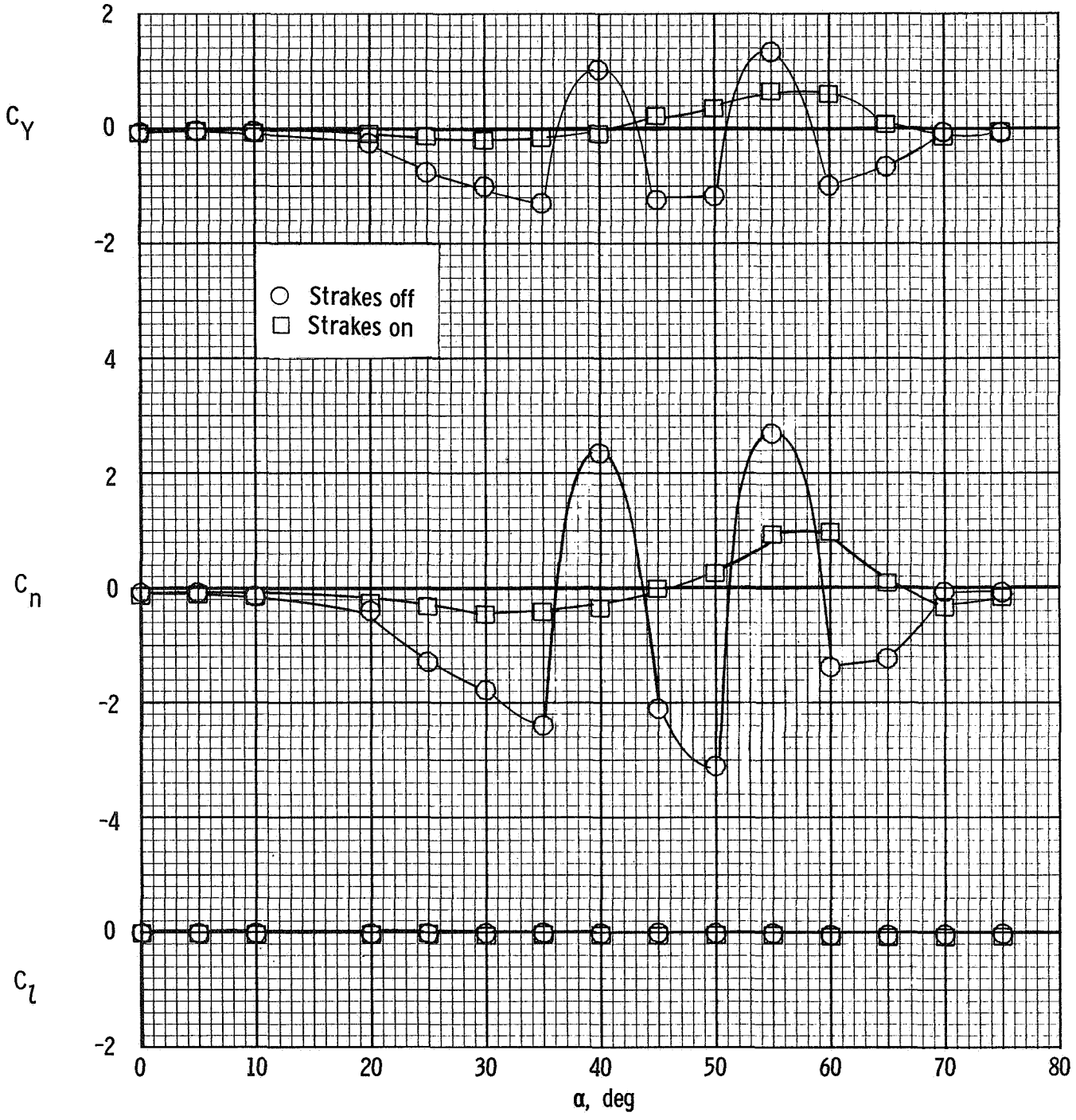

(b) Cone.

Figure 24.- Concluded.

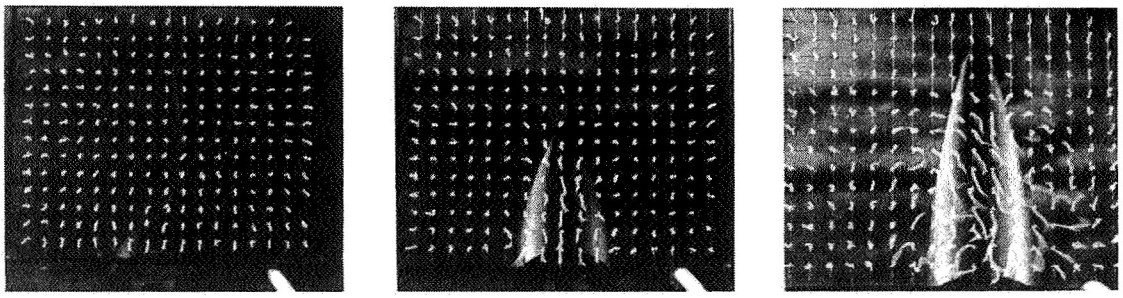

(a) Tangent-ogive model with strakes.

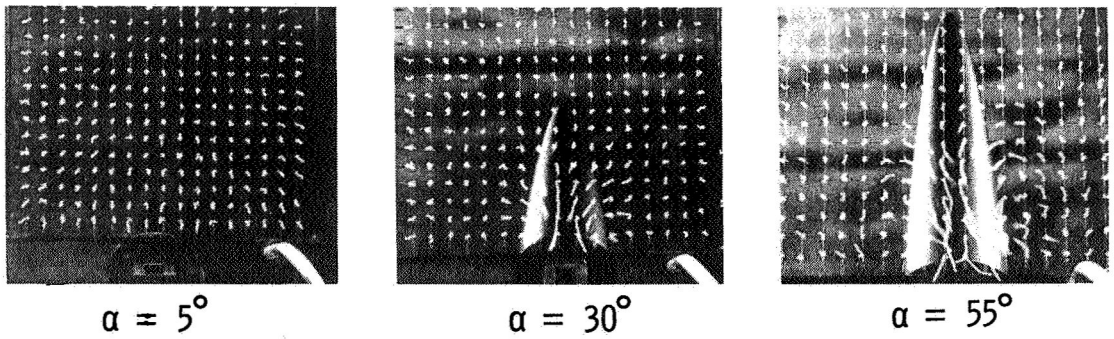

(b) Paraboloid of revolution.

Figure 25.- Comparison of tuft grid photographs for tangent-ogive model with strakes and paraboloid of revolution. $\beta = 0^{\circ}$.